Rock Physics of Geopressure and Prediction of Abnormal Pore Fluid Pressures Using Seismic Data

José M. Carcione
Istituto Nazionale di Oceanografia e di Geofisica Sperimentale, Trieste, Italy

and

Hans B. Helle
Norsk Hydro ASA, E&P Research Centre, Bergen, Norway

Summary

Various physical processes cause anomalous pressures of underground fluids in a petroleum province. We quantify the effect on seismic properties caused by the common mechanisms of overpressure generation such as (kerogen-to-oil and oil-to-gas conversion) disequilibrium compaction.

Fluid pressure due to kerogen-to-oil conversion in source-rock shale significantly reduces the seismic velocities and enhances the anisotropy. Attenuation and attenuation anisotropy are also strongly affected, thus further enhancing the seismic visibility of overpressure in the shale.

In deeply buried reservoirs, oil-to-gas cracking may increase the fluid pressure to reach the lithostatic pressure, and the seismic velocities decrease significantly when only a small fraction of oil in a closed reservoir is converted to gas.

Non-equilibrium compaction generates abnormal pressures that, under certain conditions, can be detected with seismic methods. In this case, the fluid mixture filling the pore space has a major influence on P-wave velocity and may cause under- or over-pressures depending on its compressibility and thermal expansion coefficient. Rocks saturated with fluids of low compressibility and high thermal expansion are generally over-pressured and can be seismically visible.

Based on a generalized Biot-Gassmann model for the acoustic properties of shaley sandstones, with an arbitrary pore fill mixture of fluid and gas, we have developed a new method for estimating fluid pressure in reservoir rocks from seismic data. The method which rely upon calibration against well data or laboratory data, when available, has been applied to a deeply buried overpressured gas-field in the Norwegian North Sea using velocities obtained from 3-D reflection tomography.

1. Introduction

Abnormal pressure, or pressures above or below hydrostatic pressure, occurs on all continents in a wide range of geological conditions. Various physical processes cause anomalous pressures in an underground fluid. The most commonly cited mechanisms for abnormal pressure generation in petroleum provinces are compaction disequilibrium and hydrocarbon generation including oil-to-gas cracking (Mann and Mackenzie, 1990; Luo and Vasseur, 1994). In young (Tertiary) deltaic sequences, compaction disequilibrium is the dominant cause of abnormal pressure. In older (pre-Tertiary) lithified rocks, hydrocarbon generation and tectonics are most often cited as the causes of overpressure (Law et al, 1998).

Hydrocarbon accumulations are frequently found in close association with abnormal pressure. In exploration for hydrocarbons and exploitation of the reserves, knowledge of the pressure distribution is of vital importance for prediction of the reserves, for the safety of the drilling and for optimising the recovery rate. Moreover, drilling of deep gas resources is hampered by high risk associated with unexpected overpressure zones. Knowledge of pore pressure using seismic data, as for instance from seismic-while-drilling techniques, will help producers plan the drilling process in real-time to control potentially dangerous abnormal pressures.

In order to illustrate the physics of geopressure, let as review the main concepts (see Figure 1.1). *Pore pressure*, also known as formation pressure, is the *in situ* pressure of the fluids in the pores. The pore pressure is equal to the *hydrostatic pressure* when the pore fluids only support the weight of the overlying pore fluids (mainly brine). The *lithostatic* or *confining pressure* is due to the weight of overlying sediments, including the pore fluids. In the absence of any state of stress in the rock, the pore pressure attains lithostatic pressure and the fluids support all the weight. However, fractures perpendicular to the minimum compressive stress direction

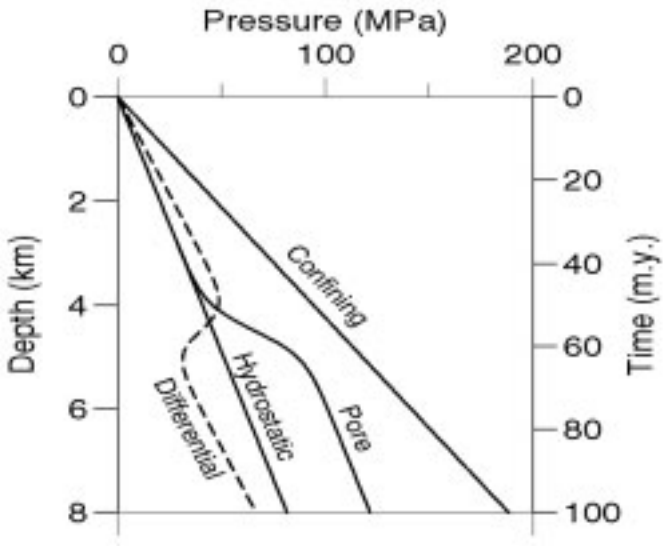

Figure 1.1: Typical pressure-depth plot where the different pressure definitions are illustrated.

Continued on Page 9

ROCK PHYSICS OF GEOPRESSURE AND PREDICTION OF ABNORMAL PORE FLUID PRESSURES USING SEISMIC DATA

Continued from Page 8

appear for a given pore pressure, typically 70-90% of the confining pressure. In this case, the fluid escapes from the pores and pore pressure decreases. A rock is said to be overpressured when its pore pressure is significantly greater than hydrostatic pressure. The difference between confining pressure and pore pressure is called *differential pressure*. As we shall see later, acoustic and transport properties of rocks generally depend on *effective pressure*, a combination of pore and confining pressures.

In deeply buried oil reservoirs, oil-to-gas cracking may increase the pore pressure to reach or exceed the lithostatic pressure (Chaney, 1950; Barker, 1990; Luo and Vasseur, 1996). Oil can be generated from kerogen-rich source rocks and flow through a carrier bed to a sandstone reservoir rock. Excess pore-fluid pressures in sandstone reservoirs are generated when the rate of volume created by the transformation of oil to gas is more rapid than the rate of volume loss by fluid flow. If the reservoir is sealed on all sides by an impermeable shale or limestone, then the condition of a *closed system* will be satisfied for gas generation. Due to the presence of semi-vertical fault planes and compartmentalization, this condition holds for most North Sea reservoirs.

Non-equilibrium compaction or mechanical compaction disequilibrium is a consequence of a rapid deposition compared to the rate of expelling pore fluids by gravitational compaction. In this situation, the fluids carry part of the load that would be held by grain contacts and abnormal pore pressures develop in the pore-space. A description of this overpressure mechanism is given by Rubey and Hubbert (1959) and mathematical treatments of the problem are provided, for instance, by Bredehoeft and Hanshaw (1968), and Smith (1971) and Dutta (1983). These models use Darcy's law and their predictions are greatly affected by the choice of the constitutive relations between porosity, permeability and effective stress.

Experimental data shows that Poisson's ratio is a good indicator of overpressure, since in gas-saturated rocks Poisson's ratio decreases with increasing pore pressure, while it increases in liquid-saturated rocks (Dvorkin and Walls, 2000). These properties are used by Carcione and Cavallini (2002) to design an algorithm for predicting pore pressure from seismic data.

Pressure compartments are common in sedimentary basins (Chiarelli and Duffaud, 1980; Bradley and Powley, 1994; Law et al., 1998). Their knowledge is extremely important to the drilling engineer to prevent blowouts and/or lost circulations. Pressure compartments can be subdivided into two different classes: those created by disequilibrium compaction and characterized by large volumes of low permeability rock; and those bounded by seals, which are formed by a combination of low permeability effects (e.g., shales) and high capillarity pressure due to the interfacial tension between two fluids (Iverson et al., 1994). Pressure compartments are bounded by pressure seals. Unlike pure capillary seals, which permit the flow of the wetting phase (brine), a pressure seal restricts both hydrocarbon and brine flow.

Effective stress and effective pressure play an important role in rock physics. The use of this concept is motivated by the fact that pore pressure, p, and confining pressure, p_c, tend to have opposite effects on the acoustic and transport properties of the rock. Thus, it is convenient to characterize those properties with a single pressure, the effective pressure p_e. Terzaghi (1936) proposed $p_e = p_c - \phi p$, where ϕ is the rock porosity, but his experiments, regarding the failure of geological materials, indicated that $p_e = p_c - p$. Nowadays, it is well known that effective pressure takes the form $p_e = p_c - np$, where n is the effective stress coefficient (Biot, 1962; Todd and Simmons, 1972; Carcione, 2001, p. 224). Biot's theory predicts an effective stress coefficient $n = 1 - K_m/K_s$, where K_m is the bulk modulus of the dry frame and K_s is that of the elastic solid from which the frame is made. It is found that $n \approx 1$ for static measurements of the compressibilities (Zimmerman, 1991), while n is approximately linearly dependent on the differential pressure $p_d = p_c - p$ in dynamic experiments (Gangi and Carlson, 1996; Prasad and Manghnani, 1997).

In general, non-seismic methods to predict pore pressure are based on a relation between porosity or void ratio and effective stress (Bryant, 1989; Audet, 1996; Traugott, 1997; Holbrook et al, 1995). Indirect use of velocity information involves the estimation of the porosity profile by using sonic-log data (Hart et al., 1995; Harrold et al., 1999). A MWD (measurement while drilling) technique is proposed by Lesso and Burgess (1986), based on mechanical drilling data (rock strength computed from ROP (rate of penetration), weight on bit (DWOB) and torque (DTOR)) and gamma ray logs.

Hydrocarbon reservoirs are generally overpressured. This situation can, in principle, be characterized by seismic waves. To this end, the dependence of the P-wave and S-wave velocities on effective stress plays an important role. Seismic data can be used to predict abnormal pore pressures in advance of drilling. In general, this prediction has been based on normal move-out analysis (e.g., Bilgeri and Ademeno, 1982) and empirical models relating pore pressure to seismic properties. In order to obtain the acoustic properties, such as wave velocity and attenuation factor, versus pore and confining pressures, the dry-rock bulk and rigidity moduli, K_m and μ_m, should be evaluated as a function of the effective pressure. Then, an appropriate model, such as Biot's theory (Biot, 1962; Carcione, 2001, p. 219-293), can be used to obtain the properties of the saturated porous medium. Those moduli can be obtained from laboratory measurements in dry samples or from well data.

The procedure is to fit the experimental data by exponential-like functions (e.g., Zimmerman, 1991, p. 43). Knowing the effective-stress coefficients for K_m and μ_m (from Biot's theory or obtained from well or laboratory data), it is possible to obtain the wave velocities for different combinations of the pore and confining pressures, since the property should be constant for a given value of the effective pressure. This is achieved by simply

Continued on Page 10

ROCK PHYSICS OF GEOPRESSURE AND PREDICTION OF ABNORMAL PORE FLUID PRESSURES USING SEISMIC DATA

Continued from Page 9

replacing the confining pressure by the effective pressure. An example of the application of this approach can be found in Carcione and Gangi (2000a,b), where the effects of disequilibrium compaction and oil to gas conversion on the seismic properties are investigated. Use of high-frequency (laboratory) data to make predictions in the seismic — low-frequency — band should be considered with caution, since the fluid effects on wave velocity and attenuation depend on the frequency range (e.g. Pham et al., 2002).

Louis and Asad (1994) used a modeling technique to analyze the amplitude variations with offset (AVO) of pressure seals. Acoustic synthetic seismograms based on well logs showed that a strong AVO effect is associated with steep pressure and velocity gradients. Carcione (2000a) considers a rock-physics model relating pressure and temperature to wave velocity and studies amplitude variations with offset of pressure-seal reflections. The model relates pore pressure to the seismic properties of a closed rock volume (the compartment). Carcione investigates the AVO response of pressure seals consisting of interbedded shale and sandstone units. The pressure model assumes that the pores are filled with oil, gas and brine. Balancing volume fractions in the pore-space yields the fluid saturations and the porosity versus pore pressure, as a function of the initial (hydrostatic) saturations and porosity (Berg and Gangi, 1999; Carcione, 2001, p. 227-229). Laboratory experiments on dry and saturated samples, for different confining and pore pressures, provide the rock moduli versus effective pressure. The AVO response of the seal is obtained by computing the reflection coefficient of a set of transversely isotropic layers (the seal) embedded between two isotropic half-spaces (the rock units above and below the seal).

The effect of clay and frequency on the acoustic properties (mainly velocity dispersion and attenuation) can be modeled by using a micro-structural theory where all the relevant physical quantities can be taken into account. The model developed by Pham et al. (2002) establishes a relation between wave velocity and attenuation and clay content, porosity, pore and confining pressures, frequency, and pore-fluid saturation. Modeling the acoustic properties of shaley sandstones is achieved by using the theory developed by Carcione et al. (2000) in the framework of Biot's theory of poroelasticity. Unlike previous theories, this approach uses a Biot-type three-phase theory that considers the existence of two solids (sand grains and clay particles) and a fluid. The theory has been generalized to include the effects of pore pressure, partial saturation and the presence of dissipation mechanism of different nature (Pham et al., 2002). Pressure effects are introduced by using an effective stress law. The effect of partial saturation on velocity and attenuation depends on the frequency range. At low frequencies, the fluid has enough time to achieve pressure equilibration (relaxed regime). In this case, the Reuss model for the bulk modulus of the fluid mixture yields results that agree with the experiments. On the other hand, at high frequencies the fluid can not relax and this state of unrelaxation induces a stiffening of the pore material, which increases the wave velocity considerably (Cadoret et al., 1995). This effect implies an uneven distribution of fluids in the pore-space, which is normally termed patchy saturation. In this case, Reuss' model is not appropriate and, in general, a Hill average is used to model the wave velocities at ultrasonic (laboratory) frequencies. No microstructural theory is able to predict the behavior at intermediate frequencies. A modified empirical fluid mixing law, proposed by Brie et al. (1995), gives the Reuss modulus at low frequencies and the Voigt modulus at high frequencies.

Attenuation is described by using a constant-Q model for the dry-rock moduli (Kjartansson, 1979; Carcione, 2001, p. 73). This approach is phenomenological, since a theory describing all the attenuation mechanisms present in a real sandstone is difficult, if not impossible, to develop. The constant-Q kernel is the simplest model based on only one parameter. We assume that the lower the frame modulus, the lower the quality factor is (that is, the higher the attenuation). Using this property, we assign a Q-factor to the sandstone bulk modulus, and obtain the Q-factor associated with the shear modulus. The Biot attenuation mechanisms are modeled by the original theory (Carcione et al., 2000), and, high-frequency viscodynamic effects are described by an optimal viscodynamic function obtained by Johnson et al. (1987).

As stated in previous works (Carcione and Gangi, 2000a,b), the large change in seismic velocity is mainly due to the fact that the dry-rock moduli are sensitive functions of the effective pressure, with the largest changes occurring at low differential pressures. The major effect of porosity changes is implicit in the dry-rock moduli. Explicit changes in porosity and saturation are important but have a lesser influence than changes in the moduli. In this sense, porosity-based methods can be highly unreliable. In fact, variations of porosity for Navajo sandstone, Weber sandstone and Berea sandstone, are only 1.7%, 7% and 4.5%, respectively, for changes of the confining pressure from 0 to 100 MPa (Berryman, 1992). The bulk and shear moduli of the sand and clay matrices versus porosity are obtained from a relationship proposed by Krief et al. (1990). To obtain the expression of the dry-rock moduli versus effective pressure, the model requires calibration based on well, geological and laboratory data, mainly sonic and density data, and porosity and clay content inferred from logging profiles.

Oil can also be extracted from shales, which can be overpressured (Matusevich et al, 1997; Berg and Gangi, 1999). In this case, overpressure takes place by conversion of kerogen to oil. Carcione (2000b) obtains a model for source-rocks relating seismic anisotropy (in velocity and attenuation) to kerogen content, pore pressure and water saturation. Recent petrophysical analyses of petroleum source-rocks (Vernik and Landis, 1996) indicate that the observed strong velocity anisotropy can be associated with the presence of organic matter and its distribution in the rock matrix. Most hydrocarbon source-rocks are laminated structures composed of organic matter (kerogen and

Continued on Page 12

ROCK PHYSICS OF GEOPRESSURE AND PREDICTION OF ABNORMAL PORE FLUID PRESSURES USING SEISMIC DATA

Continued from Page 10

oil) and illite layers. When the seismic wavelength is much larger than the thickness of the single layers, the finely layered medium behaves as a homogeneous transversely isotropic material, whose stiffnesses can be obtained using Backus averaging technique (Schoenberg and Muir, 1989). Assuming that the illite and the organic material are attenuating media, a generalization of the averaging technique to the dissipative case gives not only the wave velocities (Vernik and Nur, 1992; Vernik, 1994) but also the dissipation factors as a function of organic matter and propagation direction.

The maturation level of source-rocks can be associated with oil generation and overpressuring (e.g., Meissner, 1978). If the conversion rate is more rapid than the rate of volume loss by fluid flow, excess pore pressure is generated. A typical situation in the North Sea source-rocks is represented by the Kimmeridge shale, a source-rock from the Draupne formation, with a maximum thickness of nearly 200 m, overlain by high velocity chalk. The observed velocity contrast and thickness make the Kimmeridge shale an easily identified seismic unit. P-wave velocity and quality factor of the hydrocarbon source-rock (normal and parallel to the bedding plane) are calculated as a function of organic content and pore pressure.

We illustrate the use of the concepts mentioned above by predicting pore pressure in a North-Sea reservoir using seismic and well data. In general, this prediction has been based on empirical models relating pore pressure to sonic and/or seismic velocity (Dutta an Levin, 1990; Foster and Whalen, 1966; Pennebaker, 1968; Eaton, 1976; Belotti and Giacca, 1978; Bilgeri and Ademeno, 1982; Keyser et al., 1991; Kan and Sicking, 1994; Bowers, 1995; Eaton and Eaton, 1997; Sayers et al., 2000). Here we use the Biot-type three-phase theory developed by Carcione et al. (2000). At low frequencies, this theory is a generalization of Gassmann's equation for shaley sandstones, based on first physical principles. The method requires high-resolution velocity information, preferably obtained from seismic inversion techniques. As is well known, interval velocities obtained from conventional seismic processing are not reliable enough for accurate pore pressure prediction (Sayers et al., 2000; Carcione and Tinivella, 2001). Calibration of the model requires well information, that is, porosity and shale volume estimation, direct measurements of pore pressure and sonic-log data. Laboratory measurements of P- and S-wave velocities on cores samples may further improve the calibration process (Carcione and Gangi, 2000a,b).

2. Mechanisms of overpressure generation and the effect on seismic properties.

In order to find the appropriate relationships between underground fluid pressure and seismic properties, we first investigate the impact of the main pressure generating mechanisms on the petrophysical characteristics of source-rock shales and sandstones.

Hydrocarbon generation from source-rocks

The maturation level of a source-rock can be associated with oil generation and overpressuring (e.g., Meissner, 1978). If the conversion rate is more rapid than the rate of volume loss by fluid flow, excess pore pressure is generated. Berg and Gangi (1999) developed a simple model to calculate the excess pore pressure Δp as a function of the fraction of kerogen F converted to oil:

$$\Delta p = \frac{(\rho_k / \rho_o - 1)\, F}{c_p + c_k - F\left[c_p + c_k - (\rho_k / \rho_o)(c_p + c_o)\right]}, \qquad (2.1)$$

where ρ_k and ρ_o are the densities of kerogen and oil, respectively, and c_p, c_k and c_o are the pore, kerogen and oil compressibilities.

A typical situation in the North Sea is represented by the Draupne Formation (Figure 2.1), a Kimmeridge source-rock shale, with a maximum thickness of about 200 m, overlain by a high velocity chalk (Vernik, 1995). Between the overlying chalk and the hydrocarbon source-rock, the P-wave velocity drops from about 4.5 to 3.5 km/s (normal to the bedding plane) and density from 2.75 to 2.35 g/cm^3, producing the strongest regional seismic marker at Jurassic level in the North Sea.

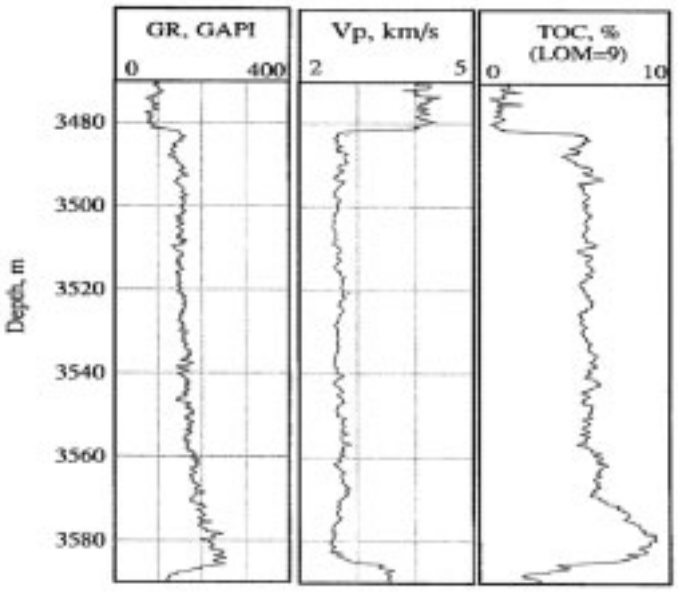

Figure 2.1: Log responses of the Draupne Formation, Viking Graben (Vernik, 1995).

Carcione (2000b) use Berg and Gangi's model for computing the material properties of the organic matter (kerogen/oil mixture), and thus the phase velocities and quality factors of the source-rock versus initial kerogen content and excess pore pressure (see Figures 2.2 and 2.3).

Continued on Page 13

ROCK PHYSICS OF GEOPRESSURE AND PREDICTION OF ABNORMAL PORE FLUID PRESSURES USING SEISMIC DATA

Continued from Page 12

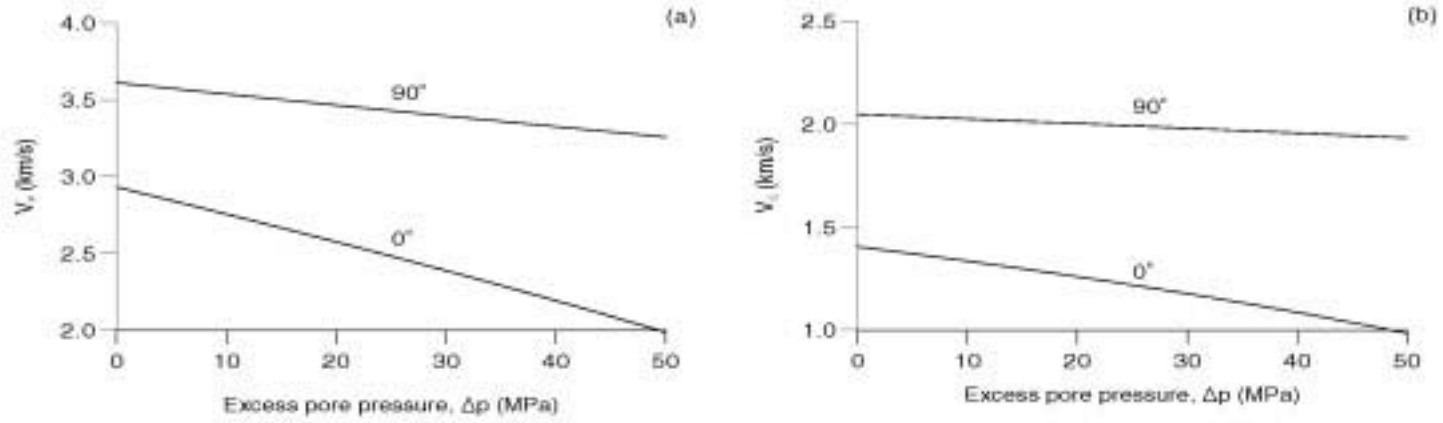

Figure 2.2: Bedding-normal velocities (0°) and bedding-parallel velocities (90°) for the compressional (a) and shear (b) waves for an initial kerogen content of 35%.

Composite model of the source-rock

Following Vernik and Nur (1992), Carcione (2000b) assumed that the immature rock is a two-layer composite made of illite and kerogen, with no additional pore fluid for the immature source-rock. Carcione considers illite transversely isotropic, kerogen isotropic, and both viscoelastic. The Backus averaging gives a transversely isotropic equivalent medium. For the source-rock under maturation the fluid (oil) is assumed to be included in the isotropic kerogen, while the anisotropic illite component remains dry.

Immature source-rock

Kerogen, in the Kimmeridge shale investigated by Vernik (1995), is mostly type II organic matter (e.g., see Vernik, 1994). Therefore, the rock is in an early maturation stage, with no hydrocarbons. Since illite has a lenticular textural pattern, only the stiffnesses "parallel to bedding" are affected. Following Vernik and Nur (1992), Carcione (2000b) modifies the stiffnesses using an equation which incorporate the respective local constants of both illite and kerogen. The modelled phase velocities and anisotropy parameters as a function of kerogen content provides a fairly good fit to the experimental values. The data show that the shale is substantially anisotropic, with positive anisotropy parameters ε and γ, which is characteristic of laminar transversely isotropic composites. Maximum stiffness anisotropy is obtained for a kerogen content of approximately 30 %.

Having calibrated the model with experimental data, it is possible to analyse the anisotropic dissipation characteristics of the source-rock versus kerogen content. The quality factor at 90° corresponding to the horizontally polarised shear wave, is dominated by the illite dissipation, while the (rapidly decreasing) quality factor at 0° is dominated by the kerogen dissipation. Maximum attenuation anisotropy is obtained for a kerogen content of approximately 18 %, compared to the 30 % for stiffness anisotropy. Thus, in the range of the experimental kerogen saturation, attenuation anisotropy can be an important indicator of the presence of kerogen, with shear wave anisotropy γ greater than 2.

From immature to mature source-rock

The different maturation stages of a source rock can be modelled by evaluating the kerogen/oil conversion and the excess pore pressure. Using certain assumptions, a simple equation relating these quantities is obtained. Knowing the fraction of kerogen converted to oil, we can compute the properties of the kerogen/oil mixture by using the model of Kuster and Toksöz (1974), and then the properties of the source-rock as a function of the excess pore pressure. Wave velocities versus excess pore pressure are represented in Figure 2.2, where an initial kerogen content of 35 % has been assumed. The bedding-normal velocities decrease more rapidly than the parallel velocities, implying higher anisotropy parameters with increasing pore pressure. The quality factors, represented in Figure 2.3, show a different behaviour; while $Q(0°)$ decreases for both waves, $Q(90°)$ increases with pore pressure, causing a significant attenuation anisotropy at high pressures.

This study demonstrates that anisotropy of wave velocity and attenuation can be used as indicators for the detection of kerogen-rich shales having different maturation levels. These levels depend on the pressure change due to oil generation in low-permeability source-rocks. The conclusions, for the North Sea Kimmeridge shale, can be summarized as follows:

- In the presence of kerogen-to-oil conversion, excess pore pressure occurs. This process simulates the different maturation levels. At the same value of the conversion factor, the excess pressure is higher in rigid rocks. For instance, for a Kimmeridge shale with 35 % kerogen content, the pore pressure necessary to reach fracture is 48 MPa, with about 28 % of the kerogen converted to oil. At this pressure, the porosity increase is approximately 10 % of the initial porosity.
- The anisotropy parameters increase and the velocities decrease with increasing kerogen-to-oil conversion and excess pore pressure. Normal-bedding quality factors decrease, but parallel quality factors increase slightly with kerogen content.

Continued on Page 14

ROCK PHYSICS OF GEOPRESSURE AND PREDICTION OF ABNORMAL PORE FLUID PRESSURES USING SEISMIC DATA

Continued from Page 13

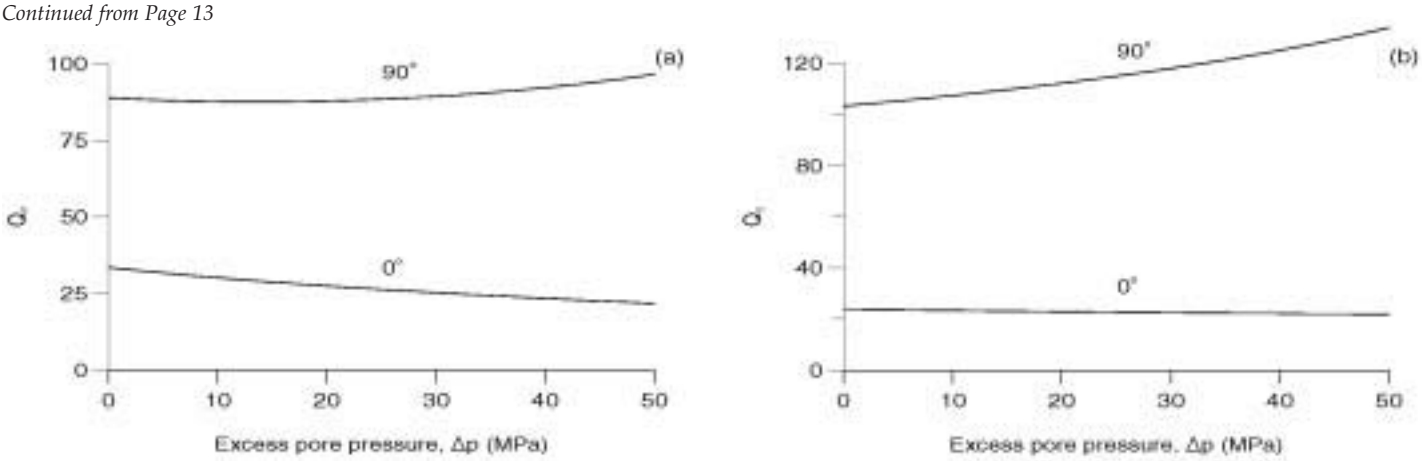

Figure 2.3: Bedding-normal (0°) quality factors and bedding-parallel (90°) quality factors for the compressional (a) and shear (b) waves for an initial kerogen content of 35 %.

- The polar anisotropy, i.e., variations with respect to the propagation direction, is more pronounced at high pore pressures.
- Increasing kerogen content and pore pressure increases the seismic visibility of the shale. The impedance contrasts calculated with the bedding-normal velocities are more sensitive than those computed with the parallel-bedding velocities.

Extension of this investigation to a more realistic situation considers the presence of water (Carcione, 2000b) and the conversion of oil to gas. Moreover, it is known that pore-volume compressibility increases greatly as the pore pressure approaches the fracture pressure (Zimmerman, 1991). The role of temperature is also important. For instance, there is experimental evidence that the compressional to shear velocity ratio increases with temperature when measured in the direction normal to bedding (Vernik and Nur, 1992).

Overpressure due to oil-gas conversion

In deeply buried oil reservoirs, oil-to-gas cracking may increase the pore pressure to reach or exceed the lithostatic pressure (Chaney, 1950; Barker, 1990; Luo and Vasseur, 1996). Oil can be generated from kerogen-rich source-rocks and flow through a carrier bed to a sandstone reservoir rock. If the reservoir is sealed on all sides by an impermeable shale or limestone, then the condition of a closed system will be satisfied for gas generation. Due to the presence of semi-vertical fault planes and compartmentalization, this condition holds for most North Sea reservoirs.

Berg and Gangi (1999)'s model can be used to calculate the excess pore pressure as a function of the fraction of kerogen converted to oil and the fraction of oil converted to gas. We use an extended version of this model for computing the porosity variations and fluid saturations as a function of the excess pore pressure (Carcione and Gangi, 2000b). Let us assume a reservoir at depth z and the lithostatic pressure for an average sediment density, $\bar{\rho}$ is equal to $p_c = \bar{\rho} g z$, where g is the acceleration of gravity. On the other hand, the hydrostatic pore pressure is approximately $p_H = \rho_w g z$, where ρ_w is the density of water. For a constant sediment burial rate, S, and a constant geothermal gradient, G, the temperature variation of a particular sediment volume is $T = T_0 + G z$, $z = St$, with a surface temperature at time $t = 0$. Typical values of G range from 20 to 30 °C/km, while S may range between 0.05 and 0.5 km/m.y. (m.y. = million years). The mass of convertible oil changes with time t at a rate proportional to the mass present. Assuming a first-order kinetic reaction (Luo and Vasseur, 1996; Berg and Gangi, 1999) and a reaction rate following the Arrhenius equation, the oil-to-gas conversion factor F can be obtained as a function of temperature and deposition time (Carcione and Gangi, 2000b).

The excess pore pressure at depth z is $\Delta p = p - p_H$, where p_H is the hydrostatic pore pressure and p is the pore pressure when a fraction F of oil has been converted to gas ($F = 0$ and $p = p_i - p_H$ at time t_i). Compressional and shear wave velocities depend on effective pressure $p_e = p_c - np$, where n is the effective stress coefficient. We assume the following functional form for the pore compressibility c_p as a function of effective pressure p_e:

$$c_p = c_p^{\infty} + \beta \exp(-p_e / p^*), \tag{2.2}$$

that the medium is fully saturated with oil and that, before oil-gas conversion occurs, the initial pressure, p_i , is hydrostatic. Balancing mass and volume fractions in the pore-space, yields the relation between the oil-to-gas conversion factor F and the pore pressure p :

$$F = \left[\frac{D\rho_{gi}}{\rho_g(p,T)} - \exp(-c_o\Delta p + \alpha_p \Delta T)\right]^{-1} \{\exp[E(\Delta p) + \alpha_p \Delta T] - \exp(-c_o\Delta p + \alpha_p \Delta T)\}, \tag{2.3}$$

where

$$E(\Delta p) = -c_p^{\infty}\Delta p_e + \beta p^*[\exp(-p_e / p^*) - \exp(-p_{ei} / p^*)]. \tag{2.4}$$

In these equations, $D = \rho_0 / \rho_{gi}$, where ρ_0 is the oil density and ρ_{gi} is the initial gas density, obtained from the van Der Waals equa-

Continued on Page 15

ROCK PHYSICS OF GEOPRESSURE AND PREDICTION OF ABNORMAL PORE FLUID PRESSURES USING SEISMIC DATA

Continued from Page 14

tion, c_0 is the oil compressibility, α_o is the thermal expansion of oil, ΔT is the temperature increase, and α_p is the thermal expansion of the pore-space. With a surface temperature of 25 °C a temperature gradient G = 25 °C/km, a sedimentation rate S = 0.08 km/m.y. and a reservoir at $z_i = z_1$ = 2 km, we have $t_i = t_1$ = 25 m.y. and T_1 = 75 °C. After 75 m.y., the depth of burial is z_2 = 8 km, t_2 =100 m.y. and T_2 = 225 °C. On the other hand, if $\bar{\rho}$ = 2.4 g/cm^3, the confining pressure has increased from p_{c1} = 47 MPa to approximately p_{c2} = 188 MPa, and the initial pore pressure is $p_i \simeq$ 20 MPa (assuming ρ_w = 1 g/cm^3). If no conversion takes place, the final pore pressure would be the hydrostatic pressure at 8 km, i.e., approximately 78 MPa.

Experimental data for oil-saturated sandstone are available in Winkler (1985, his Figures 3 and 4, and Tables 4 and 7). The experiments on dry samples correspond to zero pore pressure. Best-fit plots of the dry-rock compressibility and shear modulus vs. confining pressure are

$$K_m^{-1}[\text{GPa}]^{-1}=0.064+0.122\ \exp(-p_c[\text{MPa}]/6.48)$$

and (2.5)

$$\mu_m^{-1}[\text{GPa}]^{-1}=13.7-8.5\ \exp(-p_c[\text{MPa}]/9.14)$$

and c_p in GPa^{-1} is given by equation (2.2), with c_p^∞= 0.155, β = 0.6 and p^* = 6.48. The pore compressibility c_p has been obtained from the dry-rock bulk modulus by assuming that the porosity is that at hydrostatic pore pressure [this approximation is supported by experimental data obtained by Domenico (1977) and Han et al. (1986)]. The best-fit plots for c_p and K_m^{-1} are illustrated in Figure 2.4. In order to obtain the moduli for different combinations of the confining and pore pressures, we should make the substitution $p_c \rightarrow p_e = p_c - n(p_H + \Delta p)$, where we assume, following Gangi and Carlson (1996), that n depends on differential pressure as $n = n_0 - n_1 p_d$, n_0 = 1, n_1 = 0.014 MPa^{-1}. This dependence of n versus differential pressure is in good agreement with the experimental values corresponding to the compressional velocity obtained by Christensen and Wang (1985) and Prasad and Manghnani (1997).

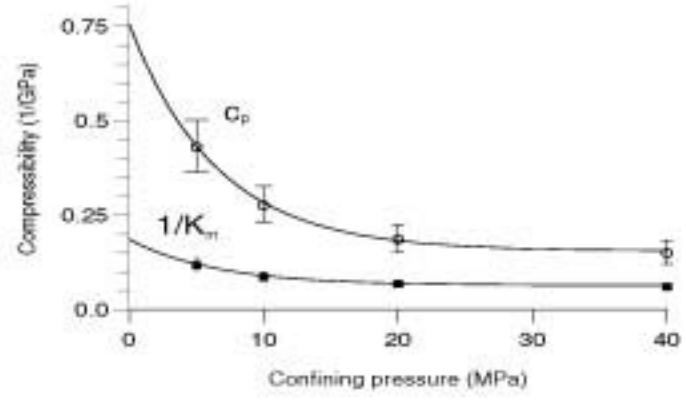

Figure 2.4: Best-fit plots of pore-space compressibility c_p and matrix bulk modulus K_m obtained from the experimental data for Berea sandstone published by Winkler (1985).

Table 2.1 indicates the properties for Berea sandstone and Table 2.2 the properties of the different fluids, with the values corresponding to the initial (hydrostatic) pore pressure. The oil density and bulk modulus are assumed pressure-independent and equal to the values indicated by Winkler (1985) for 20 MPa. The oil and gas viscosities as a function of temperature and pore pressure are taken from Luo and Vasseur (1996). Figure 2.5 shows the oil/gas conversion factor [equation (2.3)] as a function of depth and time and the pore-pressure buildup with depth. The high activation energy requires either a long time or deep burial, on the order of 4.5 to 5 km, before appreciable fractions of conversion occur, but significant fractional conversions occur at 3 km. The pressure rapidly increases for very small fractions of oil converted to gas. This is due to the low compressibility of the rock. Beyond the lithostatic pressure the effective pressure becomes negative and the pore compressibility increases (see Figure 2.4), making the rock highly compliant. This precludes a rapid increase of the pore pressure, which follows the lithostatic pressure below 4 km depth.

GRAIN	$\rho_s = 2650\ \text{kg/m}^3$ $K_s = 37\ \text{GPa}$
MATRIX	$K_m = 15.45\ \text{GPa}$ $\mu_m = 13.48\ \text{GPa}$ $\phi = 0.203$ $\mathcal{T} = 2$ $\kappa = 10^{-12}\ \text{m}^2$ $\alpha_p = 2 \times 10^{-4}\ ^\circ\text{C}^{-1}$

$1\ \text{cP} = 0.001\ \text{Pa s}$

Table 2.1: Material properties of dry Berea sandstone.

FLUID	Bulk modulus (GPa)	density (kg/m^3)	Viscosity (cP)	Thermal expansion (°C^{-1})
Light oil	0.57	700	10	5×10^{-4}
Winkler's oil	2.16	890	240	5×10^{-4}
Heavy oil	2.2	970	850	7.7×10^{-4}
Water	2.25	1040	1.8	5×10^{-4}

1 cP = 0.001 Pa s

Table 2.2: Properties of pore fluids.

Biot's theory successfully describes the wave propagation properties of synthetic porous media such as sintered glass beads. In natural porous media such as sandstone, discrepancies between Biot's theory and measurements are due to complex pore shapes that are not present in simple synthetic media (Gist, 1994). Skeleton-fluid mechanisms are modeled by generalizing the coupling modulus to a time dependent relaxation function, based on the generalized linear solid with L dissipation mechanisms (Carcione, 2001, p. 69). The mixture organics/water behaves as a composite fluid with properties depending on the constants of the constituents and their relative concentrations. The low-frequency

Continued on Page 16

ROCK PHYSICS OF GEOPRESSURE AND PREDICTION OF ABNORMAL PORE FLUID PRESSURES USING SEISMIC DATA

Continued from Page 15

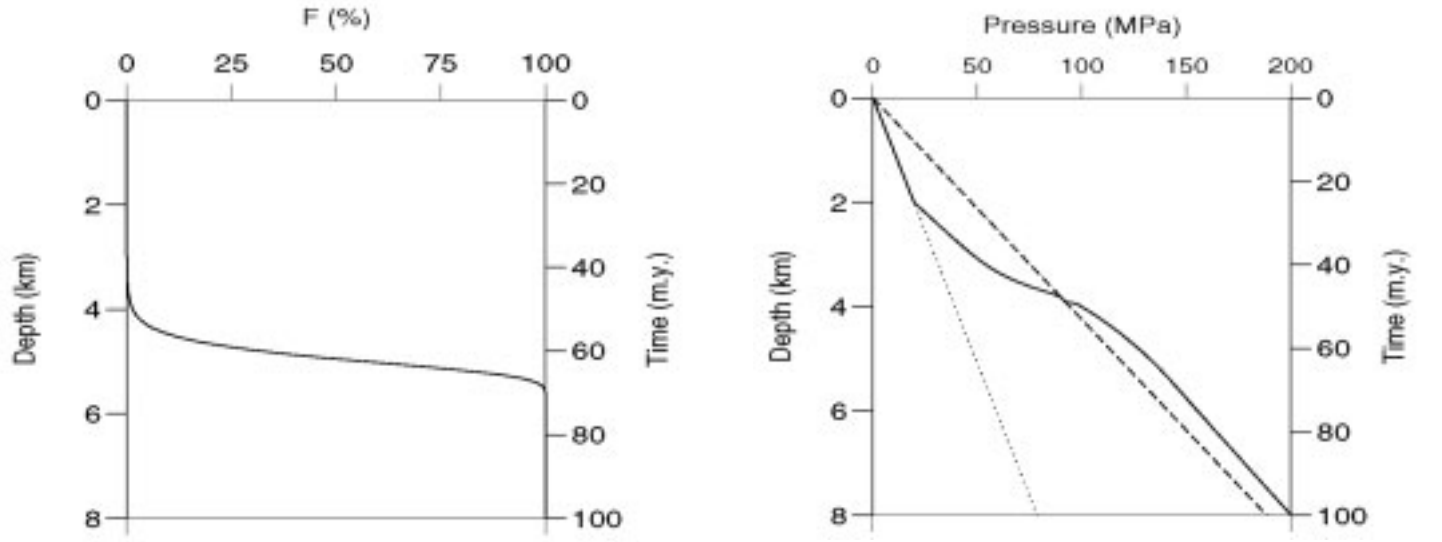

Figure 2.5: Oil/gas conversion factor as a function of burial depth at a constant sedimentation rate and constant geothermal gradient (left) *and the corresponding pressure build* (right). *Pore-pressure build-up with depth and deposition time (continuous line). The hydrostatic and lithostatic pressure is represented by dotted and broken lines respectively. Fluid pressure reaches lithostatic pressure when only 2.5% of the oil in the closed reservoir is converted to gas.*

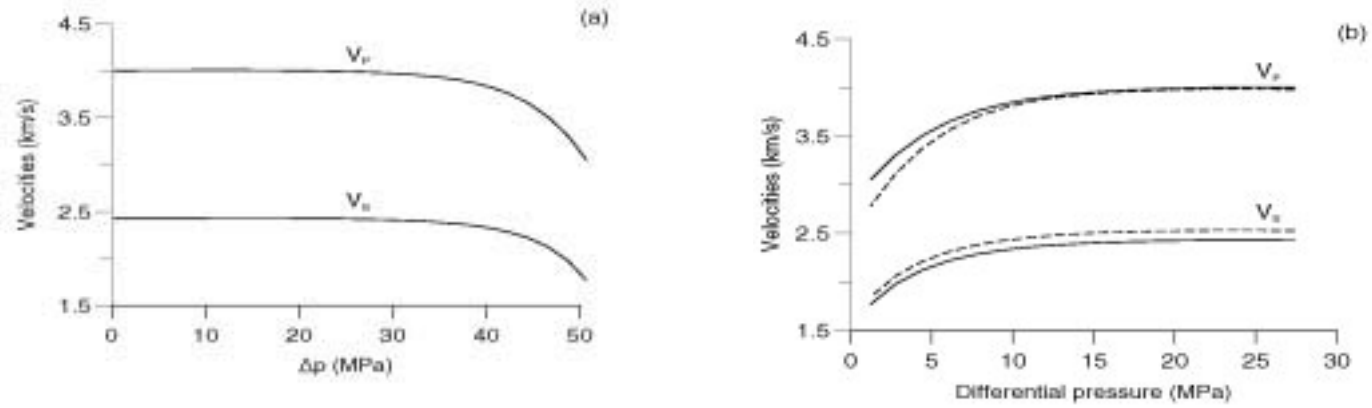

Figure 2.6: Low-frequency wave velocities versus excess pore pressure (a) and differential pressure (b). Frequency is 25 Hz. The broken lines in (b) are the dry-rock wave velocities.

wave velocities versus excess pore pressure and differential pressure for this model are shown in Figure 2.6. An excess pore pressure of 50 MPa corresponds to zero differential pressure. The oil/gas conversion starts at a differential pressure of 27.4 MPa, which corresponds to an onset time of approximately 25 million years, when the sandstone is fully saturated with oil. As can be appreciated, the velocities decrease substantially after an excess pore pressure of approximately 35 MPa. This is partially due to the replacement of oil by gas at high oil saturations, but mainly to the decrease in the matrix bulk moduli K_m and μ_m caused by the decrease in effective pressure.

Abnormal pressure due to disequilibrium compaction

The case of non-equilibrium compaction is that in which the sedimentation rate is so rapid that the pore fluids do not have a chance to 'escape'. We assume that the pore-space is filled with organic material and water, that the compressibilities of the organics and water are independent of pressure and temperature, and that of the rock is independent of temperature but depends on pressure. At time t_i, corresponding to depth z_i, with initial hydrostatic fluid pressure $p_i = \rho_w g z_i$, the volume of rock behaves as a closed system. That is, if the unit is a shale, its permeability is extremely low, and if the unit is a sandstone, the permeability of the sealing faults is sufficiently low so that the rate of pressure increase greatly exceeds the dissipation of pressure by flow. Pore pressure excess is measured relative to hydrostatic pressure. Then, it can be shown that balancing mass and volume fractions in the pore-space yields

$$\exp[E(\Delta p)+\alpha_p \Delta T] = S_{wi}[-c_w \Delta p+\alpha_w \Delta T]+(1-S_{wi})[-c_o \Delta p+\alpha_p \Delta T], \quad (2.6)$$

where S_{wi} is the initial water saturation, c_w is water compressibility, α_w is water thermal expansion and $E(\Delta p)$ is given by equation (2.4). The solution of equation (2.6) gives the pore pressure $p = \Delta p + p_i$ as a function of depth and deposition time, with $\Delta T = T - T_i = GS(t - t_i)$, for a constant geothermal gradient and a

Continued on Page 17

ROCK PHYSICS OF GEOPRESSURE AND PREDICTION OF ABNORMAL PORE FLUID PRESSURES USING SEISMIC DATA

Continued from Page 16

constant sediment burial rate. Table 2.1 indicates the properties of dry Berea sandstone, where the values correspond to those at the initial (hydrostatic) pore pressure. The pore-fluid properties are given in Table 2.2.

The pore-pressure buildup with depth for different pore fluids is shown in Figure 2.7, where the continuous lines represent the hydrostatic and lithostatic pressures. The dotted line corresponds to full light-oil saturation, and the broken lines to full Winkler's oil saturation (label 1), partial saturation (S_{wi} = 0.5 and heavy oil) (label 2), and full heavy-oil saturation (label 3). As can be appreciated, the rock is underpressured for full light-oil saturation and increasing pore-fluid bulk modulus gives overpressure. For low compressibilities and high thermal expansion coefficients of the pore fluid, the pore pressure may exceed the lithostatic pressure. In the case of heavy oil, the cause is the high thermal expansion coefficient.

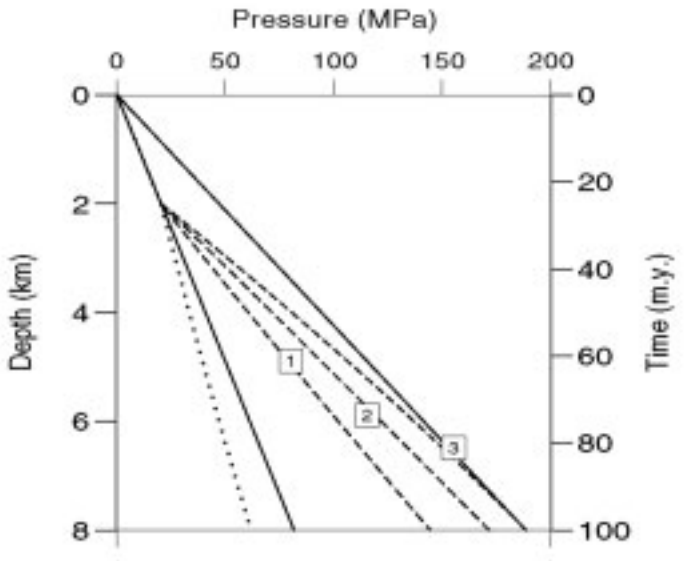

Figure 2.7: Pore-pressure build-up with depth for different pore fluids, where the continuous lines represent the hydrostatic and lithostatic pressures. The dotted line corresponds to full light-oil saturation, and the broken lines to full Winkler's (1985) heavy-oil saturation (label 1), partial saturation (S_{wi}=0.5 and heavy oil) (label 2), and full heavy oil saturation (label 3).

Figure 2.8 shows (a) the low-frequency (25 Hz) and (b) the ultrasonic (1 MHz) compressional and shear velocities versus differential pressure p_d for heavy oil (continuous line) and Winkler's oil (broken and dashed lines). The dotted line corresponds to the range 0 to 2 km, where the rock is normally pressured (see Figure 2.7); the black squares and empty circles are the experimental compressional and shear velocities obtained by Winkler (1985) for oil-saturated Berea sandstone. We use a continuous spectrum of dissipation mechanisms for the Biot's coupling modulus, from 1 Hz to 1 MHz, regardless of the saturations. The pore-fluid affects mainly the compressional velocity, with unrelaxed velocities (1 MHz) higher than relaxed velocities (25Hz), as expected. The decrease in wave velocity at low differential pressures is due to the unconsolidation effect, implicitly contained in equations (2.5). From 2 to 8 km (continuous lines) the cause is overpressuring, and from 0 to 2 km (dotted lines) the cause is the pore pressure approaching the confining pressure at very shallow depths, since in this case the rock is normally pressured. At deep depths, the wave velocities decrease substantially when the pore pressure approaches the confining pressure, as it is the case for full heavy-oil saturation.

The seismic (a) and ultrasonic (b) P-wave quality factors versus differential pressure for water-saturated Berea sandstone (S_{wi} = 1) are represented in Figure 2.9, where the black squares are the experimental values (parallel to the bedding plane) obtained by Prasad and Manghnani (1997). The low-frequency curve is obtained under the assumption of a constant quality factor from the seismic to the ultrasonic band. As before, the dotted line corresponds to the range 0 to 2 km, where the rock is normally pressured, and the continuous lines to the range 2 to 8 km, where the rock is overpressured. As wave velocities, the quality factor is not sensitive to overpressure when the pore fluid is water or

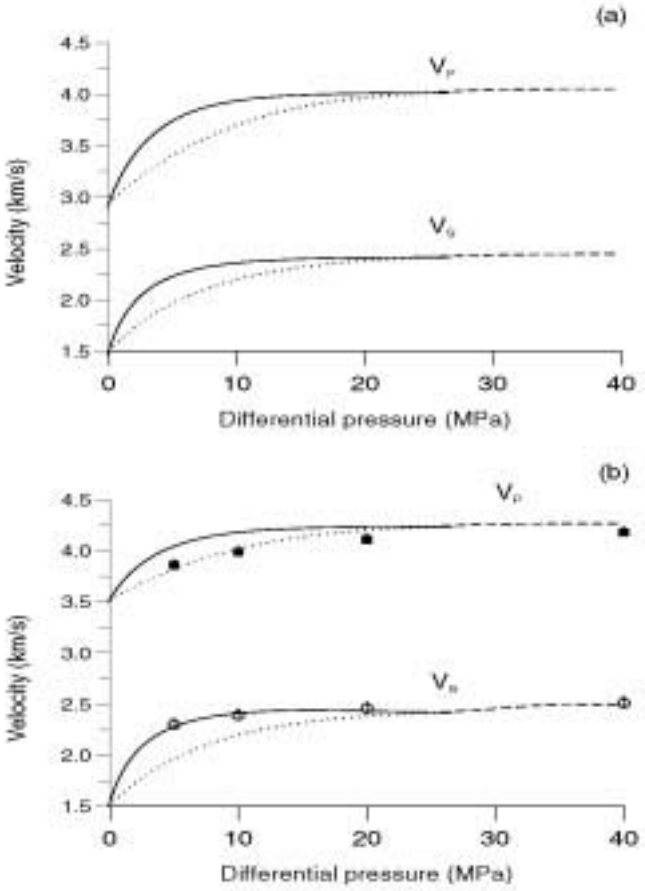

Figure 2.8: (a) Low-frequency (25 Hz) and (b) ultrasonic (1 MHz) compressional- and shear-wave velocities versus differential pressure pd for heavy oil (continuous line) and Winkler's (1985) oil (broken and dashed lines). The dotted line corresponds to the range 0 to 2 km, where the rock is normally pressured (see Figure 2.7). The black squares and empty circles are the experimental compressional- and shear-wave velocities obtained by Winkler (1985) for oil-saturated Berea sandstone. P-wave and S-wave velocities are accurate within 1% and 2%, respectively.

Continued on Page 18

ROCK PHYSICS OF GEOPRESSURE AND PREDICTION OF ABNORMAL PORE FLUID PRESSURES USING SEISMIC DATA

Continued from Page 17

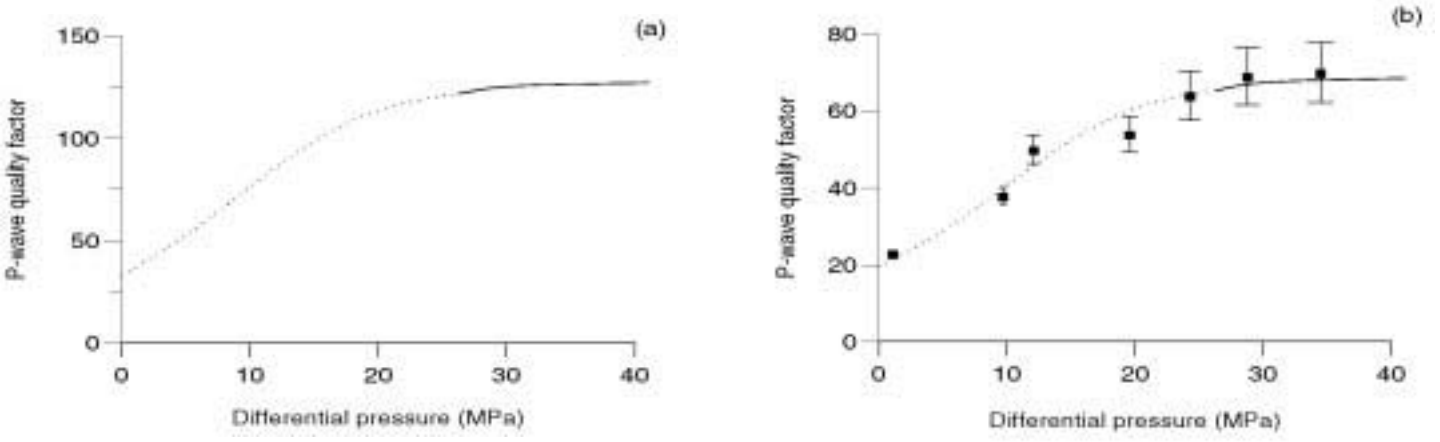

Figure 2.9: (a) Low-frequency (25 Hz) and (b) ultrasonic (1 MHz) quality factors versus differential pressure for water saturated Berea sandstone (intitial saturation Swi = 1). The black squares are the experimental bedding-parallel quality factors obtained by Prasad and Manghnani (1997) for Berea sandstone.

Winkler's oil. Overpressure implies low quality factors and therefore high wave dissipation. Quality factor can be a good indicator of excess pressure provided that reliable estimates can be obtained at seismic frequencies.

Non-equilibrium compaction generates abnormal fluid pressures that, under certain conditions, can be detected with seismic methods. This is very important in drilling applications. The results for a model in which a reservoir volume is buried at a constant sedimentation rate for a geothermal gradient, which is both constant in time and depth, show that wave velocities and quality factors decrease with decreasing differential pressure (or effective pressure). The large change is mainly due to the fact that the dry-rock moduli are functions of the effective pressure, with the largest changes occurring at low differential pressures. For a given pore-space compressibility, the fluid mixture filling the pore-space has a major influence on P-wave velocity and may cause underpressure or overpressure depending on its compressibility and thermal expansion coefficient. Rocks saturated with fluids of high compressibility and low thermal expansion coefficient are generally underpressured, and rocks saturated with fluids of low compressibility and high thermal expansion coefficient are generally overpressured, and can be seismically "visible". At high differential pressures the velocities are almost constant. Perceptible changes in the velocities occur when the differential pressure decrease to 20 MPa and become significant when the differential pressure decreases to about 15 MPa. The quality factor curve for full water saturation calculated with the present model is in good agreement with experimental values obtained at the ultrasonic frequency band. The model is able to predict pore pressure from seismic properties if reliable estimates of wave velocities and quality factor can be obtained.

3. Poro-viscoelastic representation of shaley sandstones

Modeling the acoustic properties of shaley sandstones of (V_p, V_s versus porosity, clay content and frequency) is achieved in the framework of Biot's theory of poro-elasticity. For clay/sand mixtures, such an approach requires the consideration of a medium consisting of three phases: sand, clay, and fluid. A three-phase Biot-type theory was developed by Leclaire et al. (1994) for frozen porous media. This three-phase theory assumes that there is no direct contact between sand grain and ice, implying the existence of the water layer around the grains, isolating them from the ice. The model, which predicts three compressional waves and two shear waves, has recently been applied, with some minor modifications, to modeling the acoustic properties of permafrost (Carcione and Seriani, 2001) and gas hydrates (Carcione and Tinivella, 2000).

Carcione et al. (2000) replaced ice with clay and included the terms responsible for the interaction between the sand grains (pure quartz grain) and the clay particles in the potential and kinetic energies. Lagrange's equations provide the differential equations of motion. A plane-wave analysis gives the wave velocities and attenuation factors of the different modes. The bulk and shear moduli of the sand and clay matrices versus porosity are obtained from a relationship proposed by Krief et al. (1990). This relationship introduces two empirical parameters that can be obtained by calibrating the model with real data. An additional parameter provides one more degree of freedom for adjusting the velocity-porosity curves (at constant clay content) to the data.

The model for shaley sandstones provided by Carcione et al. (2000) is somewhat similar to that recently proposed by Goldberg and Gurevich (1998). An important difference, however, is associated with the three-phase approach. Indeed, Goldberg and Gurevich (1998) assumed that the medium is composed of only two phases, solid and fluid. The solid matrix, in turn, is a composite material, made of sand grains and clay particles. The elastic moduli of the solid/fluid mixture were derived using Gassmann's equation. However, the latter is valid only when the solid matrix is homogeneous (Brown and

Continued on Page 19

ROCK PHYSICS OF GEOPRESSURE AND PREDICTION OF ABNORMAL PORE FLUID PRESSURES USING SEISMIC DATA

Continued from Page 18

Korringa, 1975). This implies that the sand and clay particles are mixed homogeneously and forming in effect composite grains, which in turn form the rock matrix. The three-phase approach is free of such assumption, but it also implies a particular topological configuration, namely the one where sand and clay form two continuous and interpenetrating solid matrices.

We consider the model of Krief et al. (1990) to obtain estimates of the dry-rock moduli K_{sm}, μ_{sm} (sand matrix), K_{cm}, μ_{cm}(clay matrix) versus porosity and clay content. The porosity dependency of the sand and clay matrices should be consistent with the concept of critical porosity, since the moduli should vanish above a certain value of the porosity (usually from 0.4 to 0.5). The theory predicts three compressional waves and two shear waves.

Due to complexity of natural rocks and its pore-fill, Biot's theory alone is not sufficient for modeling porous media. Several effects should be added and taken into considerations such as the viscodynamic effect, viscoelasticity, pressure effects, and partial saturation (Pham et al., 2002). Figures 3.1a,b compare the P- and S-wave velocities predicted with experimental data obtained by King et al. (2000). In (b), the velocities are represented for several frequencies, from the seismic to the ultrasonic band. Also shown is the P-wave velocity obtained by using Hill's equation (Mavko et al., 1998, p. 115). We average the reciprocal of the P-wave modulus (ρV_p^2) in the absence of attenuation. The use of the modified Brie et al.'s model (Pham et al., 2002)., though empirical, allows us to model the acoustic properties of the sandstone in the whole frequency range.

Three-dimensional plots of the P-wave velocity (a) and dissipation factor (b) versus differential pressure — confining pressure minus pore pressure — and water saturation are displayed in Figure 3.2. The clay content is 5 % and the frequency is 30 Hz. Note the strong decrease of the velocity and Q factor with decreasing differential pressure This effect is mainly due to the fact that the dry-rock moduli are sensitive functions of the effective pressure. (At very low effective pressures, the rock becomes unconsolidated.) Figure 3.3 shows the same properties as in Figure 3.2, but versus water saturation and frequency. In this case, the differential pressure is 40 MPa (p_c = 70 MPa and p = 30 MPa), and we assume that the temperature is 90 °C in van der Waal's equation (Carcione and Gangi, 2000b), corresponding to a reservoir at 3 km depth. Figure 3.3b agrees qualitatively with a similar plot — based on experimental data of Massilon sandstone —published by Murphy (1982). The dissipation factor has a maximum value at the Biot relaxation peak, ranging from sonic frequencies for gas (S_w = 0) to ultrasonic frequencies for water saturated rock with a peak value around S_w = 0.8. The latter behaviour agrees with experimental data published by Yin et al. (1992).

4. Seismic-to-pressure conversion

The sand/clay acoustic model for shaley sandstones, developed by Carcione et al. (2000) yields the seismic velocities as a function of clay (shale) content, porosity, saturation, dry-rock moduli, and fluid and solid-grain properties. As stated before, the large change in seismic velocity is mainly due to the fact that the dry-rock moduli are sensitive functions of the effective pressure, with the largest changes occurring at low differential pressures. The major effect of porosity changes is implicit in the dry-rock moduli. Explicit changes in porosity and saturation are important but have a lesser influence on wave velocities than changes in the moduli. This is due to the fact that the moduli are highly affected by the contact stiffnesses between grains. In this sense, porosity-based methods can be highly unreliable.

In order to use the theory to predict pore pressure, we need to obtain the expression of the dry-rock moduli versus effective pressure. The calibration process should be based on well, geological and laboratory data, mainly sonic and density data, and porosity and clay content inferred from logging profiles.

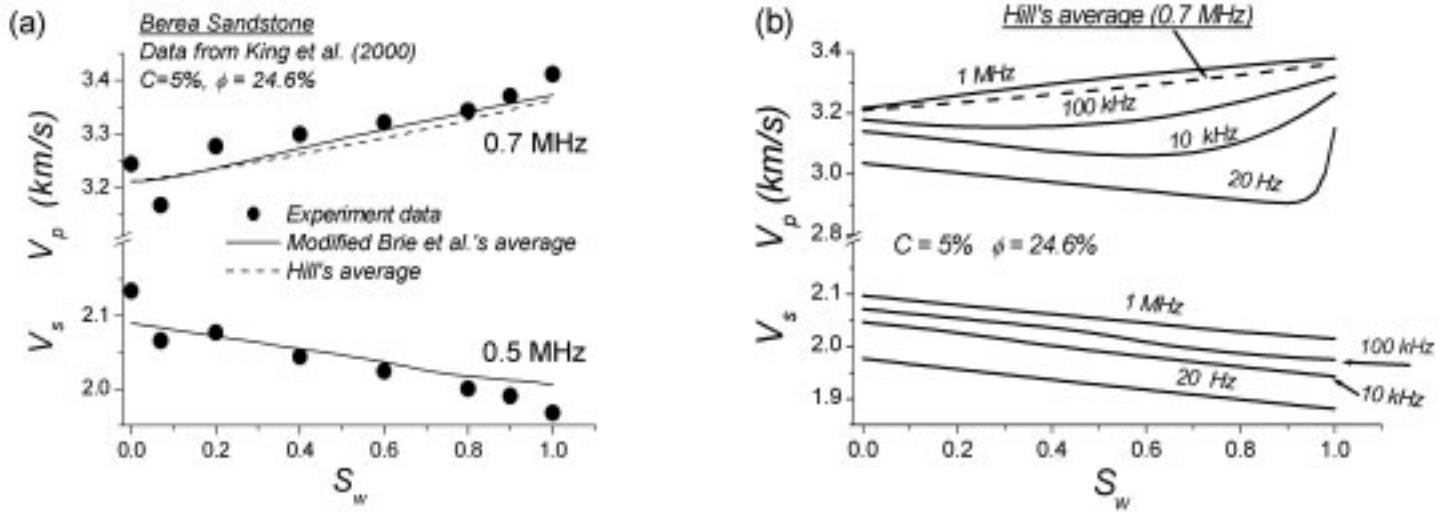

Figure 3.1: (a) P- and S-wave velocities vs water saturation predicted by the present model compared to the experimental data of King et al. (2000) at ultrasonic frequencies. (b) The same properties as in (a), but for all frequencies. Also shown, is the P-wave velocity obtained by using Hill's equation.

Continued on Page 20

ROCK PHYSICS OF GEOPRESSURE AND PREDICTION OF ABNORMAL PORE FLUID PRESSURES USING SEISMIC DATA

Continued from Page 19

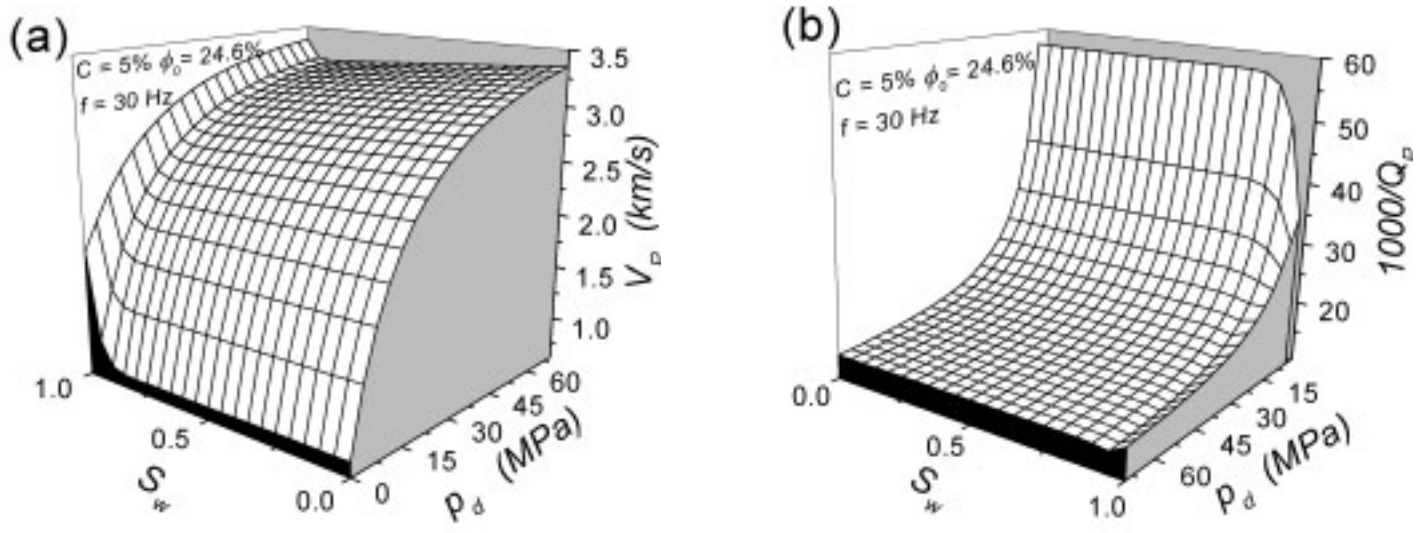

Figure 3.2: The P-wave velocity (a) and dissipation factor (b) as function of differential pressure and water saturation for seismic frequencies (30 Hz).

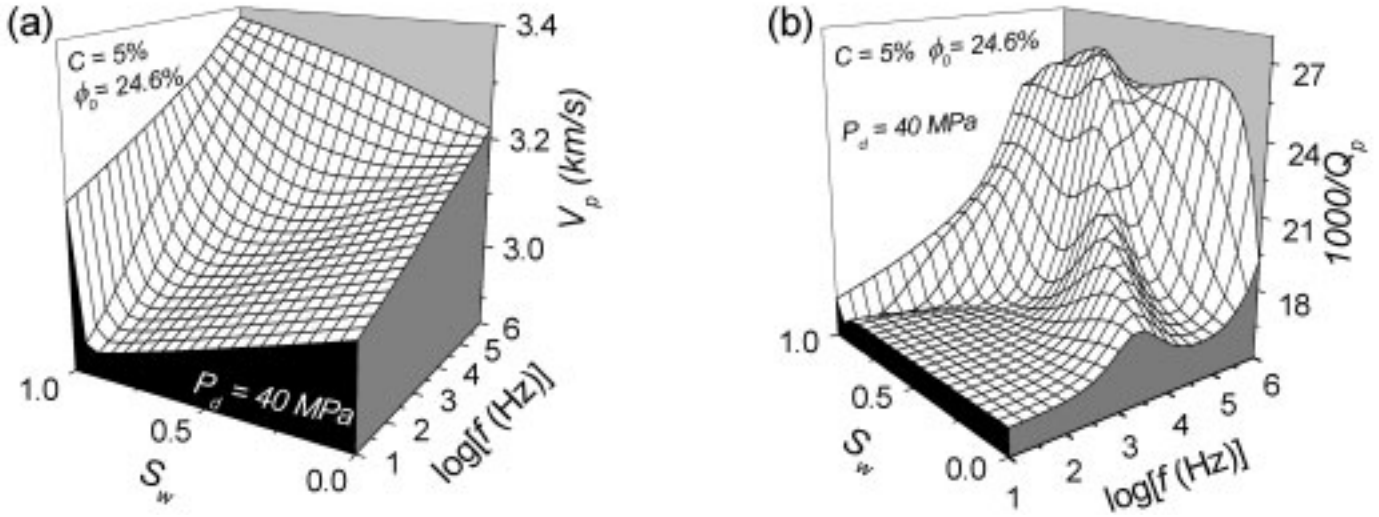

Figure 3.3: Three-dimensional plots of the P-wave velocity (a) and dissipation factor (b) versus water saturation and frequency at constant differential pressure p_d = 40 MPa.

Let us assume a rock at depth z. The lithostatic or confining pressure can be obtained by integrating the density log. We have that

$$p_c = g\int_0^z \rho(z')dz', \qquad (4.1)$$

where ρ is the density and g is the acceleration of gravity. Furthermore, the hydrostatic pore pressure is approximately given by $p_h = g\rho_w z$, where ρ_w is the density of water. As a good approximation (Prasad and Manghnani, 1997), compressional- and shear-wave velocities and bulk and shear moduli depend on effective pressure $p_e = p - np$, where p is the pore pressure and n is the effective stress coefficient, which can be different for velocities and moduli. Note that the effective pressure equals the confining pressure at zero pore pressure.

In general, n is approximately linearly dependent on the differential pressure $p_d = p_c - p$ in dynamic experiments (Gangi and Carlson, 1996; Prasad and Manghnani, 1997). Therefore, we assume $n = n_1 - n_2 p_d = n_1 - n_2(p_c - p)$. This dependence of n versus differential pressure is in good agreement with the experimental values, corresponding to the compressional velocity obtained by Christensen and Wang (1985) and Prasad and Manghnani (1997). It is clear that to obtain n_1 and n_2, we need two evaluations of n at different pore pressures, preferably a normally pressured well and an overpressured well. If one well or equally pressured wells are available, the algorithm provides an average value for n.

Calibration of the model

Ideally, a precise determination of n requires laboratory experiments on saturated samples for different confining and

Continued on Page 21

ROCK PHYSICS OF GEOPRESSURE AND PREDICTION OF ABNORMAL PORE FLUID PRESSURES USING SEISMIC DATA

Continued from Page 20

pore pressures. However, even this "laboratory" n does not reflect the behaviour of the rock at the in-situ conditions, due to two main reasons. First, laboratory measurements of wave velocity are performed at ultrasonic frequencies, and second, the in-situ stress distribution is different from the stress applied in the experiments. In the absence of laboratory data, or for shales, we perform the following steps with the data available from a calibration well (see Figure 4.2):

1. We use Krief et al.'s model (Krief et al., 1990) modified by Goldberg and Gurevich (1998) to obtain the dry-rock moduli as a function of depth, using the clay-content and porosity profiles.
2. We calculate the upper limit of the dry-rock moduli — at infinite effective pressure — using the Hashin-Shtrikman (HS) upper bounds (Hashin and Shtrikman, 1963), and assume an exponential law for the bulk moduli versus effective pressure.
3. We compute the exponential coefficients (see equation (4.3)) using the values of the moduli obtained in step 1, the confining and (measured) pore pressures, and the effective stress coefficients predicted by Biot's theory.
4. We obtain the in-situ effective stress coefficients by fitting the theoretical wave velocities (Carcione et al., 2000) to the sonic-log wave velocities, using the dry-rock moduli versus effective pressure obtained in steps 2 and 3, and n as a fitting parameter. The effective stress coefficient versus pore pressure, corresponding to the same geological unit, is obtained by using the linear law $n = n_1 - n_2 p_d$.

It is important to point out here that the HS bounds and Biot's effective stress coefficient do not depend on the size and shape of the grain and pores. In this sense, the model has a general character. The only conditions are linearity, isotropy and the low-frequency approximation.

If sandstone cores are available, we proceed as follows:

- The upper limits (infinite confining pressure) and exponential coefficients of the moduli are obtained by fitting the dry-rock moduli, which are calculated from the dry-rock wave velocities, while n is obtained from experiments on saturated samples for different confining and pore pressures (Carcione and Gangi, 2000a,b).

Continued on Page 22

ROCK PHYSICS OF GEOPRESSURE AND PREDICTION OF ABNORMAL PORE FLUID PRESSURES USING SEISMIC DATA

Continued from Page 21

- Continue with step 4 of the preceding list. This step should improve the determination of n, estimated with laboratory experiments in step 1.

More precisely, we use the following data of the study area, to calibrate the model and obtain the effective-stress-coefficient profile for the formations under consideration:

- An estimation of the porosity profile, $\phi(z)$, to use in Krief et al's model (see below) and in the sand/clay acoustic model (from a series of logs using artificial neural networks (Helle et al, 2001)).
- An estimation of the clay-content profile $C(z)$, to use in Krief et al's model (see below) and in the sand/clay acoustic model (shale volumes obtained from well logs using neural networks (Helle et al., 2001)).
- Direct measurements of pore pressure, $p(z)$ from repeat formation tests (RFT) and/or mud weights provided by the mud-logging operator).
- Sonic-log information, that is, the P-wave and S-wave velocity profiles, $V_p(z)$ and $V_S(z)$, used to obtain n_K and n_μ for the whole range of effective pressures by fitting the theoretical wave velocities to V_p and V_S. Here, n_K and n_μ are the effective stress coefficients corresponding to the dry-rock bulk and shear moduli, respectively.

No laboratory experiments available

Firstly, we consider the model of Krief et al. (1990), to obtain an estimation of the dry-rock moduli ,K_{sm} , μ_{sm} (sand matrix), and K_{cm}, μ_{cm} (clay matrix) versus porosity and clay content. The porosity dependence of the sand and clay matrices should be consistent with the concept of critical porosity (Mavko et al., 1998, p. 244) since the moduli should vanish above a certain value of the porosity (usually from 0.4 to 0.5). This dependence is determined by the empirical coefficient A (see equation (4.2)). This relation was suggested by Krief et al. (1990) and applied to sand/clay mixtures by Goldberg and Gurevich (1998). The bulk and shear moduli of the sand and clay matrices are respectively given by

$$\begin{aligned} K_{sm} &= K_s[1-C(z)][1-\phi(z)]^{1+A/[1-\phi(z)]} \\ K_{cm} &= K_c C(z)[1-\phi(z)]^{1+A/[1-\phi(z)]} \\ \mu_{sm} &= K_{sm}(z)\mu_s/K_s \\ \mu_{cm} &= K_{cm}(z)\mu_c/K_c \end{aligned} \qquad (4.2)$$

where K_s and μ_s are the bulk and shear moduli of the sand grains, and K_c and μ_c those of the clay particles. Krief et al. (1990) set the A parameter to 3 regardless of the lithology, and Goldberg and Gurevich (1998) obtain values between 2 and 4, while Carcione et al. (2000) use A = 2. Alternatively, the value of A can be estimated by using regional data from the study area. We use a general form of Goldberg and Gurevich's equation. Experimental data is fitted in Carcione et al. (2000), showing that the model has been successfully tested. The model is not based on a dual porosity theory, but there is only one (connected) porosity. The clay moduli are taken from fit to experimental data in Goldberg and Gurevich's paper.

Secondly, we assume the following functional form for the dry-rock moduli as a function of effective pressure:

$$M(z) = \alpha(z)\left[1-\exp\left(-p_e(z)/p^*(z)\right)\right] \qquad (4.3)$$

where $\alpha(z)$, and $p^*(z)$ should be obtained (for each moduli) by fitting Krief et al's expressions (4.2). The effective pressure at depth z is assumed to be $p_e = p_c - n_0 p$, where p_c is given by equation (4.1), p is given, and n_0 is a first estimation of the effective stress coefficient, based on Biot's theory (Todd and Simmons, 1972; Zimmerman, 1991, p. 33).

Since there are two unknown parameters ($\alpha(z)$, and $p^*(z)$) and one value of M for each depth, $\alpha(z)$ is assumed to be equal to the Hashin-Shtrikman (HS) upper bounds (Hashin and Shtrikman, 1963, Mavko et al., 1998, p.106). Note that the HS lower bounds are zero, and that the Voigt bounds are $(1-\phi)\ K_s$ and $(1-\phi)\mu_s$, respectively. For quartz grains with clay, K_s = 39 GPa and μ_s = 33 GPa (Mavko et al., 1998, p. 307), and if the limit porosity is 0.2, the HS upper bounds for the bulk and shear moduli are 26 GPa and 22 GPa, compared to the Voigt upper bounds 31 GPa and 26 GPa, respectively. However, the HS bounds are still too large to model the moduli of in-situ rocks. These contain clay and residual water saturation, inducing a chemical weakening of the contacts between grains (Knight and Dvorkin, 1992; Mavko et al., 1998, p. 203).

Figure 4.1 shows the dry-rock bulk modulus of several reservoir rocks for different confining pressures (Zimmerman, 1991, p. 29, Table 3.1), compared to the HS upper bounds. The solid line represents the analytical curve (4.4). On the basis of these data we apply a constant weight factor β = 0.8 to the HS bounds — due to the softening effects.

Equation (4.3) for the sand matrix can be written as

$$K_{sm}(z) = \beta K_{HS}(z)\left[1-\exp(-p_e(z)/p_K^*(z))\right], \qquad (4.4)$$

and

$$\mu_{sm}(z) = \beta\mu_{HS}(z)\left[1-\exp(-p_e(z)/p_\mu^*(z))\right]. \qquad (4.5)$$

where we assume that the effective stress coefficients are given by Biot's expressions (Todd and Simmons, 1972),

$$\begin{aligned} & n_{0K}(z) = 1-K_{sm}(z)/K_s \\ \text{and} \quad & n_{0\mu}(z) = 1-\mu_{sm}(z)/\mu_s = n_{0K}(z) \end{aligned} \qquad (4.6)$$

and p_e depends on the specific coefficient. The last equality

Continued on Page 23

ROCK PHYSICS OF GEOPRESSURE AND PREDICTION OF ABNORMAL PORE FLUID PRESSURES USING SEISMIC DATA

Continued from Page 22

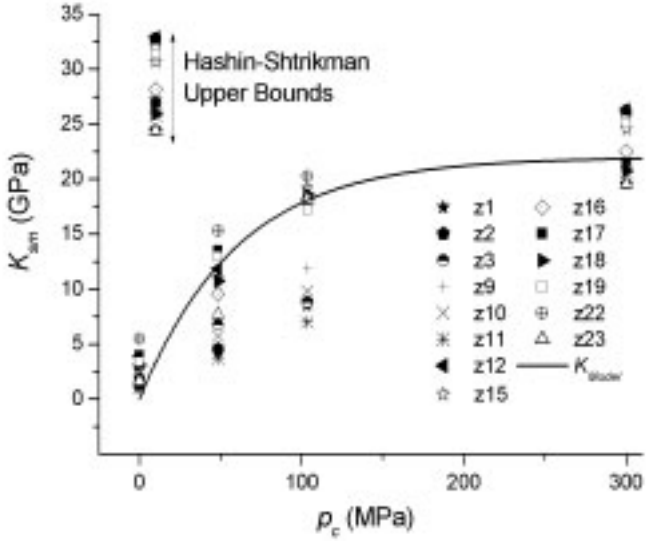

Figure 4.1: Dry-rock bulk modulus of several reservoir rocks for different confining pressures, compared to the HS upper bounds. The solid line represents the analytical curve (4.4). The data (z1-z23) is taken from table 3.1 of Zimmerman (1991).

results from the third equation(4.2), and the second equation is merely an extension of the first to the case of shear deformations.

Laboratory experiments available

The evaluation can be improved if laboratory data of dry-rock P-wave and S-wave velocity are available, and serves to constrain the values of α and p^* in equation (4.3). These sparse calibration points are based on sandstone or shaley sandstone cores, since dry measurements in shales are practically impossible to perform. The seismic bulk moduli K_{sm} and μ_{sm} versus confining pressure can be obtained from laboratory measurements in dry samples. If $V_p(dry)$ and $V_s(dry)$ are the experimental compressional and shear velocities, the moduli are given approximately by

$$K_{sm} = (1-\phi)\rho_s\left(V_P^2(dry) - \frac{4}{3}V_S^2(dry)\right)$$
and
$$\mu_{sm} = (1-\phi)\rho_s\left(V_S^2(dry)\right) \qquad (4.7)$$

where ρ_s is the grain density. We recall that K_{sm} is the rock modulus at constant pore pressure, i.e. the case when the bulk modulus of the pore fluid is negligible compared with the dry-rock bulk modulus, as for example air at room conditions. Then, we perform experiments on saturated samples for different confining and pore pressures, to obtain the effective stress coefficient n. Because these experiments yield the P-wave and S-wave velocities, and the effective stress coefficients of wave velocity and wave moduli may differ from each other, we obtain n for

$$K = \rho\left(V_P^2 - \frac{4}{3}V_S^2\right), \text{ and } \mu = \rho V_S^2 \qquad (4.8)$$

where K and μ are the undrained moduli.

Calculation of the effective stress coefficients

The last step of the calibration process is to consider equation $p_e = p_c - np$ and obtain the effective stress coefficients $n_K(z)$ and $n_\mu(z)$ by fitting the theoretical velocities to the corresponding sonic-log P-wave and S-wave velocities, by using expressions (4.3). First, we obtain n_μ by fitting the S-wave velocity, because this velocity only depends on μ_{sm}, and then, we obtain n_K by fitting the P-wave velocity. If shear-wave velocity data is not available, we assume $n_\mu = n_{0\mu}$, i.e., the Biot estimate. From the values of n obtained at the two wells, we obtain the linear law for the geological unit under investigation. The values of clay content and porosity away from the wells are assumed to be equal to those of the nearest well. Interpretation is required to follow the geological units laterally, as a function of depth, so that the n profiles can be properly extrapolated. In this study, the clay-matrix modulus is simply given by Krief et al's expressions, respectively, with no explicit dependence on pressure.

Pore-pressure calculation

Finally, the seismic velocity, derived from velocity analysis and inversion techniques, can be fitted with the theoretical velocities by using the pore pressure as fitting parameter. The theory (Carcione et al., 2000) allows us to introduce different kinds of information explicitly, such as composition (clay content), fluid saturation, porosity, permeability and viscosity (Pham et al., 2002). Before dealing with the seismic data we should test the above procedure in a nearby over-pressured well. The pore pressure prediction flow chart is shown in Figure 4.2 (Carcione et al., 2001, 2002).

AVO-based verification

In some cases, velocity information alone is not enough to distinguish between a velocity inversion due to overpressure and a velocity inversion due to pore fluid and lithology (e.g., base-of-salt reflections (Miley, 1999; Miley and Kessinger, 1999)). There are cases, where overpressuring is not associated with large velocity variations, as in smectite/illite transformations. Best et al. (1990) use AVO analysis to treat these cases. Modeling analysis of AVO signatures of pressure transition zones are given in Miley (1999), Miley and Kessinger (1999), Carcione (2000a,c) and Tinivella et al. (2001). This type of analysis should complement the present prediction method on the basis of geological information of the study area.

5. Application to a North Sea gas field

We consider the Tune Field area in the Viking Graben of the North Sea. This basin is 170-200 km wide, and represents a fault-bounded north-trending zone of extended crust, flanked by the mainland of western Norway and the Shetland platform. The area is characterized by large normal faults with north, northeast and northwest orientations which define tilted blocks. Such blocks contain the sequences present within the well used for

Continued on Page 24

ROCK PHYSICS OF GEOPRESSURE AND PREDICTION OF ABNORMAL PORE FLUID PRESSURES USING SEISMIC DATA

Continued from Page 23

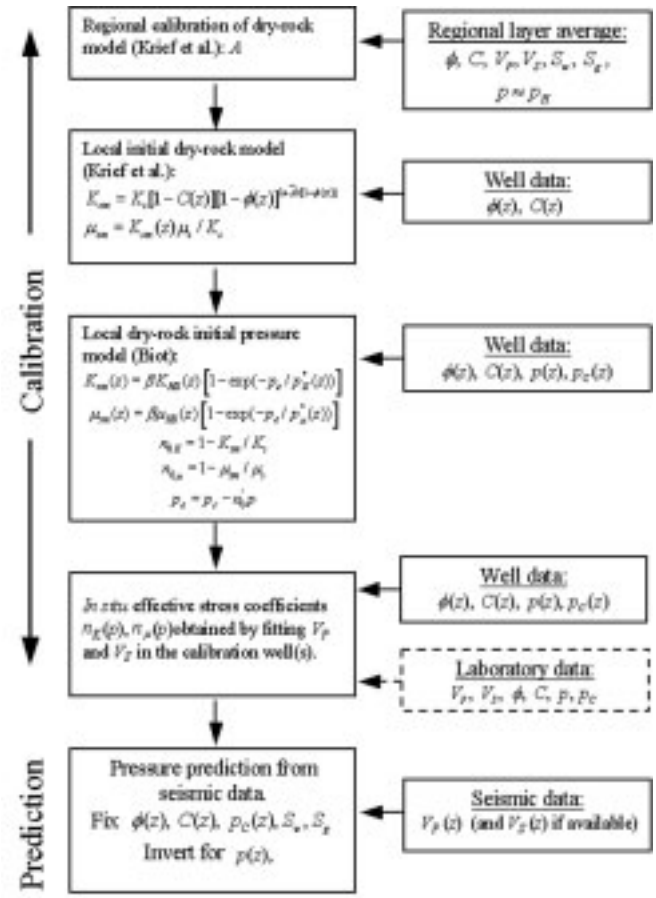

Figure 4.2: Flow chart illustrating the pore pressure prediction method from seismic data.

this study. The main motivation for selecting this area is the fact that highly overpressured compartments were identified by drilling, and that higher overpressure is expected in future wells down the flank side towards the central Viking Graben. A detailed analysis of the fault sealing and pressure distribution in Tune Field is given by Childs et al. (2002).

Figure 5.1 displays a structural time map of Top Ness, showing the pressure compartments and the locations of three wells. Well 2 and 3 are overpressured (by about 15 MPa) and well 1 has almost normal (hydrostatic) pore pressure. The dashed line indicates the location of the seismic section shown in Figure 5.2. The calibration well (well 1) is an exploration well drilled to a depth of 3720 m (driller's depth) to test the hydrocarbon potential of the Jurassic Brent Group. The well includes reservoir rocks of the Tarbert and Ness formations. The Tarbert sands are the target units considered in the present study.

The 3-D marine seismic data was acquired by using a system of 6 streamers of 3 km length with a group interval of 12.5 m and cross-line separation of 100 m. The shot spacing was 25 m and the sampling rate 2 ms. The conventional stacked section is displayed in Figure 5.2, where the location of the wells is shown.

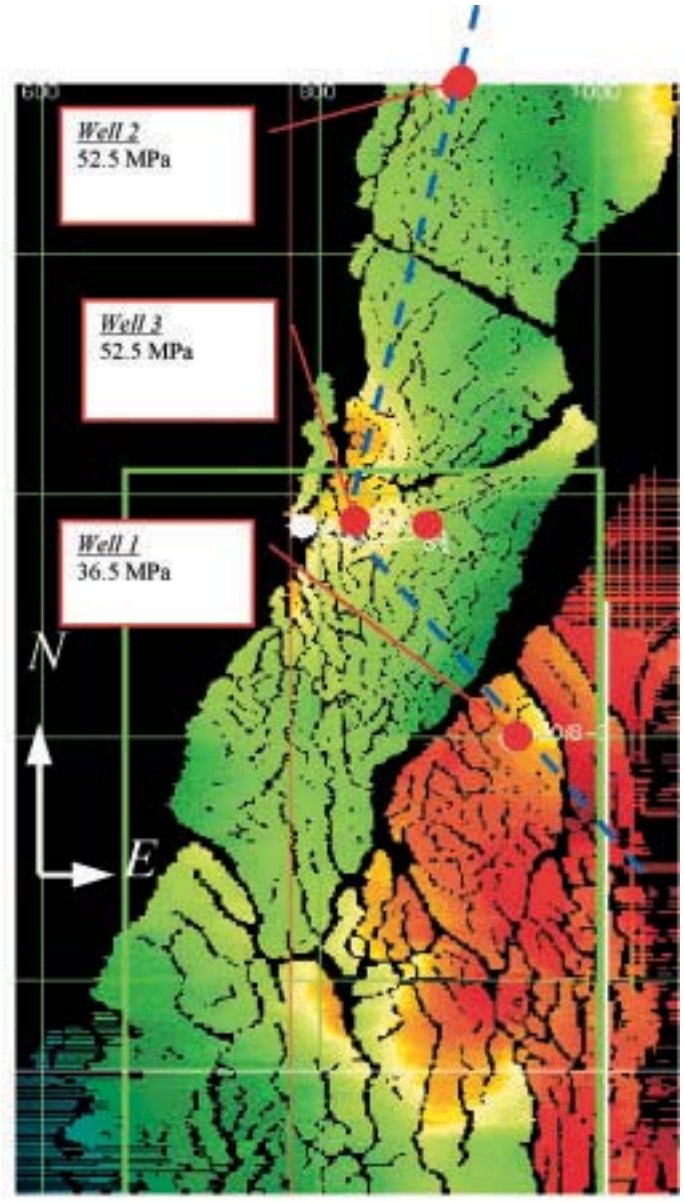

Figure 5.1: Structural time map of Top Ness (base reservoir) showing the pressure compartments in the study area. Well 2 and 3 are overpressured (by about 15 MPa). In well 1 there is almost normal (hydrostatic) pore pressure. The dashed line indicates the location of the seismic section shown in Figure 5.2. Notice that well 3 is highly deviated as indicated by the well location at surface (east) and at depth (west).

Figure 5.3 shows pressure and formation data (porosity ϕ, clay content C, density ρ, water saturation S_w and sonic-log velocities V_p and V_S) for the Tune wells. Note that well 1 is water bearing with moderate pore pressures while wells 2 and 3 are gas bearing and overpressured. Reservoir properties and fluid saturation are derived from wireline data using the neural net approach of Helle et al. (2001) and Helle and Bhatt (2002).

Velocity determination by tomography of depth migrated gathers

Recent advances in depth migration have improved subsurface model determination based on reflection seismology.

Continued on Page 25

ROCK PHYSICS OF GEOPRESSURE AND PREDICTION OF ABNORMAL PORE FLUID PRESSURES USING SEISMIC DATA

Continued from Page 24

Subsurface imaging is linked to velocity, and an acceptable image can be obtained only with a highly accurate velocity field. It has been recognized that prestack migration is a powerful velocity analysis tool that yields better imaging results than poststack migration in complicated structures. The basic assumption underlying the velocity determination methods based on prestack migration is that when the velocity is correct, all the migrations with data in different domains (e.g. different offset, different shots, different migration angles etc.) must yield a consistent image. In order to obtain the velocity field, we use the seismic inversion algorithm described by Koren et al. (1998).

We start with an initial model based on the depth converted time model, using a layer velocity cube based on conventional stacking velocities, and the interpreted time-horizons from the Tune project. Line by line, we perform the 3-D prestack depth migration using the initial velocity model and an appropriate aperture (3 km x 3 km at 3 km depth) in the 3-D cube. Through several iteration loops the model is gradually refined in velocity and hence depth. Each loop includes re-interpretation of the horizons in the depth domain, residual moveout analysis and residual moveout picks in the semblance volume. This is performed for each reflector of significance, starting at the seabed and successively stripping the layers down to the target.

The tomography considers, 1) an initial velocity model and, 2) the errors as expressed by the depth gather residual moveout and the associated 3-D residual maps. From these two inputs a new velocity model is derived where the layer depths and layer velocities are updated iteratively in order to yield flat gathers. The refined model is derived using a tomographic algorithm that establishes a link between perturbation in velocity and interface location, and traveltime errors along the common reflection point (CRP) rays traced across the model. CRP rays are ray pairs that obey Snell's law and emanate from points along the reflecting horizon, arriving at the surface with predefined offsets, corresponding to the offset locations for the migrated gathers. Each pair establishes a relationship between

Continued on Page 26

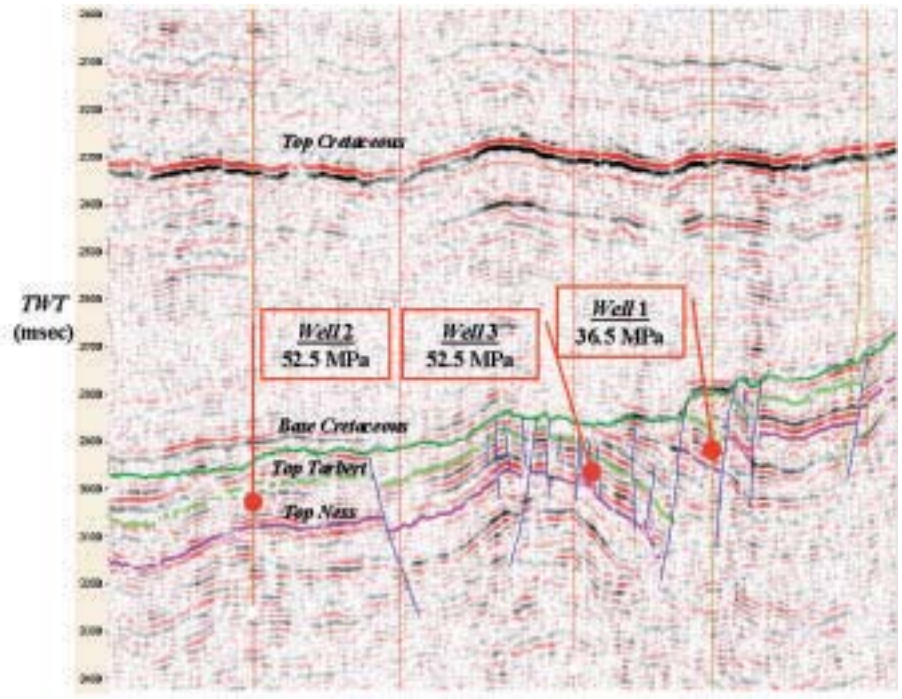

Figure 5.2: Seismic section through Tune wells (Figure 5.3) showing the location of the Top Tarbert -Top Ness interval. The mean reservoir fluid pressures are indicated. The depths of interest are between Top Tarbert (green) and Top Ness (pink).

ROCK PHYSICS OF GEOPRESSURE AND PREDICTION OF ABNORMAL PORE FLUID PRESSURES USING SEISMIC DATA

Continued from Page 25

TOMOGRAPHY #	WELL 1	WELL 2	WELL 3
1	4034	3883	3842
2	4025	3785	3825
3	4012	3777	3806
4	4004	3780	3791
5	3986	3797	3804
6	4012	3772	3803
7	4019	3782	3760
MEAN	4013	3797	3804
ST. DEV.	15	39	26

Table 5.1: Statistics of Top Tarbert-Top Ness tomography velocities (in m/s) at the well locations.

SAND	$\rho_s = 2650$ kg/m^3 $K_s = 39$ GPa $\mu_s = 33$ GPa
CLAY	$\rho_c = 2650$ kg/m^3 $K_c = 20$ GPa $\mu_c = 10$ GPa
PORE FLUIDS	$\rho_w = 1040$ kg/m^3 $K_w = 2.4$ GPa $\rho_g = 100$ kg/m^3 $K_g = 0.01$ GPa

Table 5.2: Material properties of the single constituents.

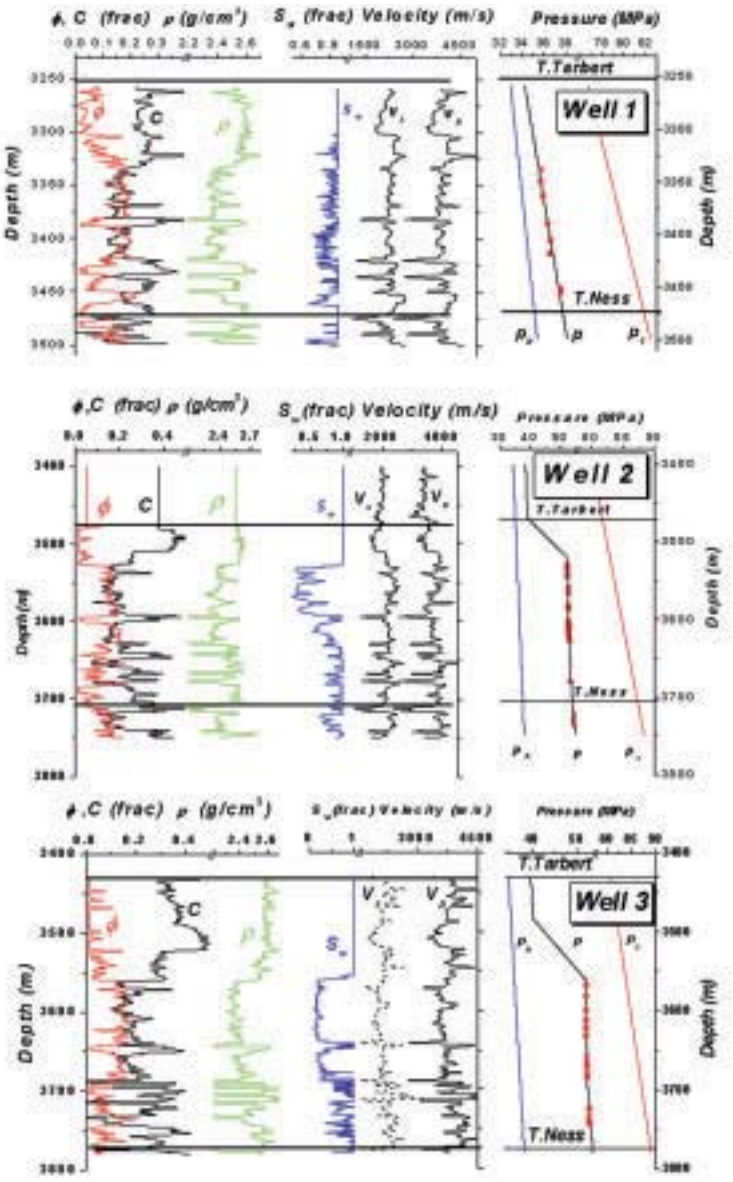

Figure 5.3: Pressure and formation data (porosity ϕ clay content C, density ρ, water saturation S_w and sonic-log velocities V_p and V_s for the Tune wells.

the CRP and the midpoint of the rays at the surface. Depth errors, indicating the difference in depth of layer images and reference depth, are picked on the migrated gather along the horizon and converted to time errors along the CRP rays. The equations relating the time errors to changes in the model are solved by a weighted least squares technique. The final model consists of seven layers, i.e., the sea water layer, seabed-Top Diapir (clay diapirism is a characteristic feature of Tertiary throughout the area), Top Diapir-Top Balder, Top Balder-Top Cretaceous, Top Cretaceous-Base Cretaceous, Base Cretaceous-Top Tarbert, and the target layer, Top Tarbert-Top Ness. The velocity maps for Top Tarbert -Top Ness is shown in Figure 5.4 (left panel), where the well locations are indicated. The Cretaceous layer velocity and the depth to Base Cretaceous reveal a remarkable similarity, i.e., where the Cretaceous is deep the velocity is high and where the Cretaceous is shallow the velocity is low, indicating that the velocity of Cretaceous is essentially governed by the overburden (e.g. compaction). Base Cretaceous, Top Tarbert and Top Ness depth maps display the more dramatic geometry of Upper Jurassic, where the Tarbert Formation is completely eroded in the northwest and where patches of missing Ness are present along the major faults. These erosion features are, of course, well reflected in the layer velocities since here the layer thickness tends to zero and layer velocity is hence not defined. Structural features are well displayed in the velocity maps of the Top Tarbert and Top Ness. The Base Cretaceous-Top Tarbert velocity map reveals, however, a fairly scattered distribution, with small patches of highs and lows within the main fault blocks.

For the reservoir itself, represented by the Top Ness velocity map, the distribution is far more coherent. In the Tarbert formation at wells 2 and 3 in the North fault block, there are consistently lower velocities than at well 1 in the East block. This feature is fairly constant for several independent velocity analysis, with a velocity

Continued on Page 27

ROCK PHYSICS OF GEOPRESSURE AND PREDICTION OF ABNORMAL PORE FLUID PRESSURES USING SEISMIC DATA

Continued from Page 26

increase of about 200 m/s across the fault separating the gas-bearing reservoir in the North block from the water-bearing reservoir in the East block. A high-velocity ridge separates the lows at well 2 and 3. Distinct low-velocity zones are also seen to the south and southeast that are not correlated with the depth variations. On the other hand, the high-velocity zones in the southwest may be related to the Tarbert dipping down at the western flank. Table 5.1 shows the results of seven independent velocity analysis obtained in the three well locations, revealing that the differences in mean velocity between the "normal" well 1 and the two overpressured wells 2 and 3 are far beyond the estimated error.

Application of the velocity model for pressure prediction

In order to estimate the pressure map in the Tarbert formation, we follow the procedure outlined above. Table 5.2 shows the values of the basic physical quantities used to compute the theoretical velocities. Gas density and gas bulk modulus are computed by using the van der Waals equation, as described in Carcione and Gangi (2000b). (The values indicated in the table are for hydrostatic pressure.) We assume, according to Biot's theory, that $n_1 = 1$, i.e., that at zero differential pressure the frame bulk modulus vanishes. The same assumption has been used for the effective stress coefficient related to the frame rigidity modulus. Figure 5.4 shows the velocity map (left panel) and the overpressure map assuming $S_w = 0.35$ and a gas saturation $S_g = 0.65$ (center panel). The picture at the right represents the difference in pore pressure by assuming gas-bearing Tarbert (the center picture) and water-bearing Tarbert (S_w= 0.94 and $S_g = 0.06$). An overpressure of about 15 MPa is predicted for well 2, while slightly higher overpressure (18 MPa) is predicted for well 3. The direct measurements indicate overpressures of about 15 MPa (see Figure 5.3). Figure 5.4 (right panel) shows that the sensitivity of the model to fluid saturation is about 8 MPa, indicating that significant uncertainity can be attributed to assumption of uniform saturation.

The velocity obtained by careful analysis of pre-stack 3-D data from the deep and complex Tarbert reservoir in the Tune gas field is sufficiently sensitive to pressure and

Continued on Page 28

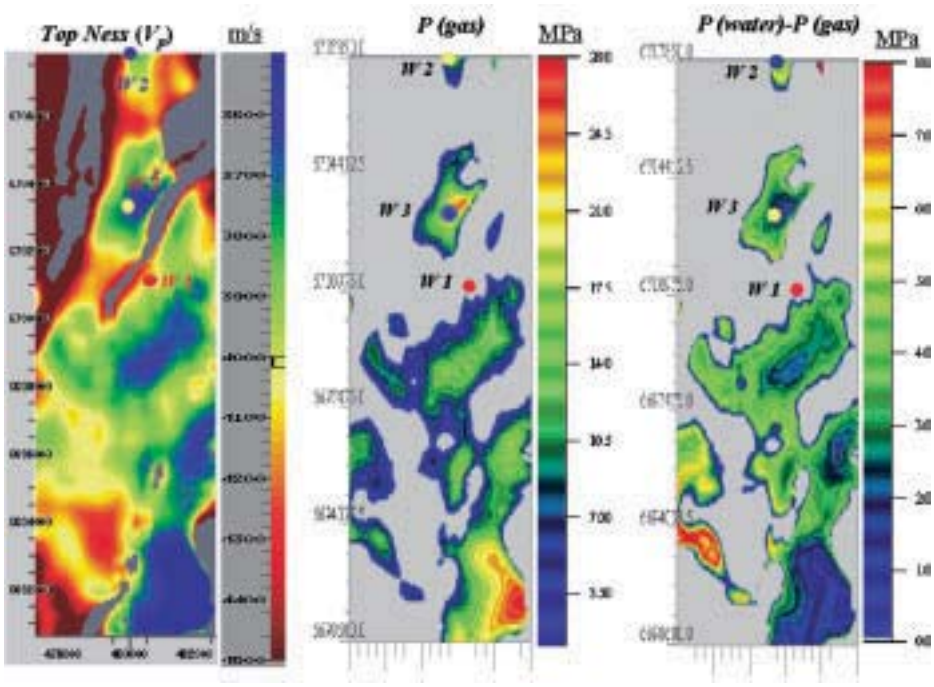

Figure 5.4: Seismic velocity map (left), overpressure prediction (center) and difference in overpressure due to gas-bearing Tarbert and water-bearing Tarbert (right).

Continued from Page 27

pore fluid to perform a meaningful analysis.The velocity and pressure distribution complies well with the structural features of the target and the general geological understanding of the pressure compartments in the Tune field. The partial saturation model used for pressure prediction can conveniently be calibrated against well data, provided that a complete set of logging data are available for the zone of interest. The most important part of the prediction process is the determination of the effective stress coefficients and dry-rock moduli versus effective pressure, since these properties characterise the acoustic behaviour of the rock. The inversion method based on the shaley sandstone model must fix some parameters while inverting the others. For instance, assuming the reservoir and fluid properties (mainly, the saturation values), formation pressure can be inverted. Conversely, assuming the pore pressure, the saturations can be obtained. The latter implies that this method may be used in reservoir monitoring where the pressure distribution is known while saturation, i.e., the remaining hydrocarbon reserves, are uncertain. We have neglected velocity dispersion, which is not easy to take into account, since *Q* factor measurements are rare and difficult to obtain with enough reliability. When using laboratory data for the calibration, the effect of velocity dispersion can be significant (Pham et al., 2002).

6. Conclusions

Abnormal pressure, or pressures above or below hydrostatic pressure, occurs on all continents in a wide range of geological conditions. In young (Tertiary) sequences, compaction disequilibrium is the dominant cause of abnormal pressure. In older (pre-Tertiary) rocks, hydrocarbon generation and tectonics are most often cited as the causes of overpressure. Hydrocarbon accumulations are frequently found in close association with abnormal pressure. Thus, in exploration for hydrocarbons and exploitation of the reserves, knowledge of the pressure distribution is of vital importance for prediction of migration routes and location reserves, for the safety of the drilling and for optimising the recovery rate in production.

In this study, we have quantified the effect on seismic properties caused by the common mechanisms of overpressure generation such as hydrocarbon generation, oil-to-gas cracking and disequilibrium compaction. Fluid pressure due to hydrocarbon generation in source-rock shale significantly reduces the seismic velocities and enhances the anisotropy. Attenuation and attenuation anisotropy are also strongly effected, thus further enhancing the seismic visibility of overpressure in the shale.In deeply buried reservoirs, oil-to-gas cracking may increase the fluid pressure to reach lithostatic pressure, and the seismic velocities are shown to drop significantly when only a small fraction of oil in a closed reservoir is converted to gas. Non-equilibrium compaction generates abnormal pressures that, under certain conditions, can be detected with seismic methods. In this case, the fluid mixture filling the pore-space has a major influence on P-wave velocity and my cause under- or over-pressures depending on its compressibility and thermal expansion coefficient. Rocks saturated with fluids of low compressibility and high thermal expansion are generally overpressured and can be seismically visible.

The feasibility of pressure prediction from seismic data rely upon two main factors:

- Accuracy of the relationships linking the rock physics parameters to pore pressure and properties of the seismic wavefield.
- The quality of the seismic data and the analysis of seismically derived parameters such as the wave velocity and amplitude (AVO).

We have attempted to link the rock physics parameters, based on first-principles, directly to pore pressure whereas the common conversion methods are based on empirical porosity-stress models valid only for shales saturated with water. Our method, on the other hand, applies to shaley reservoir rocks as well as pure sandstone and shale. Since drilling hazard more often is associated with overpressure in reservoir rocks containing gas rather than with low-permeability water saturated shale, a more general method that accounts for variation in lithology and pore-fill can be justified. However, no reliable method of pore pressure estimation from seismic data can be applied without model calibration against rock physics parameters, as obtained from well logs or laboratory experiments. In absence of local wells a calibration based on regional data is normally in favour of importing empirical relationships developed for a different basin.

Recent developments in 3-D seismic data acquisition and processing techniques have provided an appropriate platform for accurate estimation of seismic velocity and amplitude for input to the pressure analysis. This is further fertilised by the recent developments in techniques and availability of software for 3-D prestack depth migration, velocity tomography and AVO, which greatly enhance the feasibility of pore pressure estimation from seismic data.

The velocity obtained from the Tune gas field is sufficiently sensitive to pressure and pore fluid to perform a meaningful analysis. A critical step in the prediction procedure is the determination of the effective stress coefficients and dry-rock moduli versus effective pressure, since these properties characterise the acoustic behaviour of the rock. The inversion method based on the shaley sandstone model must fix some parameters while inverting the others. For instance, assuming the reservoir and fluid properties, formation pressure can be inverted. Conversely, assuming the pore pressure, the saturations can be obtained. The latter also illustrates the ambiguity imbedded in the problem that may be resolved by AVO.

Continued on Page 29

ROCK PHYSICS OF GEOPRESSURE AND PREDICTION OF ABNORMAL PORE FLUID PRESSURES USING SEISMIC DATA

Continued from Page 28

Acknowledgements

The European Union under the project "*Detection of overpressure zones by seismic and well data*" has supported a substantial part of this work.

References

Audet, D. M., 1996, *Compaction and overpressuring in Pleistocene sediments on the Lousiana shelf, Gulf of Mexico*, Marine and Petroleum Geology, 13, 467-474.

Barker, C., 1990, *Calculated volume and pressure changes during the thermal cracking of oil to gas in reservoirs*: AAPG Bull., 74, 1254-1261.

Belotti, P. and Giacca, D., 1978, *Seismic data can detect overpressure in deep drilling*, Oil and Gas Journal, August issue.

Berg, R. R., and Gangi, A. F., 1999, *Primary migration by oil-generation microfracturing in low-permeability source rocks: Application to the Austin chalk, Texas*: AAPG Bull., 83 (5), 727-756.

Berryman, J. G., 1992, *Effective stress for transport properties of inhomogeneous porous rock*, J. Geophys. Res.,97, 17409-17424.

Best, M. E., Cant, D. J., Mudford, B. S., and Rees, J. L., 1990, *Can velocity inversion help map overpressure zones? Examples from an offshore margin*, 60th Ann. Internat. Mtg., Soc. Expl. Geophys., Expanded Abstracts, 763-765.

Bilgeri, D., and Ademeno, E. B., 1982, *Predicting abnormally pressured sedimentary rocks*, Geophys. Prosp., 30, 608-621.

Biot, M. A., 1962, *Mechanics of deformation and acoustic propagation in porous media*: J. Appl. Phys., 33, 1482-1498.

Bowers, G. L., 1995, *Pore pressure estimation from velocity data, Accounting for overpressure mechanisms besides undercompaction*, IADC/SPE Drilling Conf., #27488, 515-530.

Bradley, J. S., and Powley, D. E., 1994, *Pressure compartments in sedimentary basins*: A review: AAPG Memoir 61, 3-26. The American Association of Petroleum Geologists.

Bredehoeft, J. D., and Hanshaw, B. B., 1968, *On the maintenance of anomalous fluid pressures: I. Thick sedimentary sequences*, Geol. Soc. Am. Bull., 79, 1097-1106.

Brie, A., Pampuri, F., Marsala, A. F., and Meazza, O., 1995, *Shear sonic interpretation in gas-bearing sands*, SPE Annual Technical Conf.,#30595, 701-710.

Brown, R. J. S. and Korringa, J., 1975, *On the dependence of the elastic properties of a porous rock on the compressibility of the pore fluid*: Geophysics, 40, 608-616.

Bryant, T. M., 1989, *A dual pore pressure detection technique*, SPE #18714.

Cadoret, T., Marion, D., and Zinszner, B., 1995, *Influence of frequency and fluid distribution on elastic wavevelocities in partially saturated limestones*, J. Geophys. Res., 100, 9789-9803.

Carcione, J. M., 2000a, *Amplitude variations with offset of pressure-seal reflections*, Geophysics, 66, 283-293.

Carcione, J. M., 2000b, *A model for seismic velocity and attenuation in petroleum source rocks*, Geophysics, 66, 1080-1092.

Carcione, J. M., 2000c, *AVO effects of a hydrocarbon source-rock layer*, Geophysics, 66, 419-427.

Carcione, J. M., 2001, *Wave fields in real media: Wave propagation in anisotropic, anelastic and porous media*: Handbook of Geophysical Exploration, vol. 31, Pergamon Press Inc.

Carcione, J. M. and Gangi, A., 2000a, *Non-equilibrium compaction and abnormal pore-fluid pressures: effects on seismic attributes*, Geophys. Prosp., 48, 521-537.

Carcione, J. M. and Gangi, A., 2000b, *Gas generation and overpressure: effects on seismic attributes*, Geophysics, 65, 1769-1769.

Carcione, J. M., Gurevich, B. and Cavallini, F., 2000, *A generalized Biot-Gassmann model for the acoustic properties of clayley sandstones*, Geophys. Prosp., 48, 539-557.

Carcione, J. M., Helle, H. B., Pham, N. H., and Toverud, T., 2001, *Pore pressure estimation from seismic reflection data*, EAGE/SEG Research Workshop on Reservoir Rocks, Pau, France.

Carcione, J. M., Helle, H. B., Pham, N. H., and Toverud, T., 2002, *Pore pressure estimation in reservoir rocks from seismic reflection data*, Geophysics (submitted)

Carcione, J. M. and Seriani, G. 2001, *Wave simulation in frozen sediments*: J. Comput. Phys., 170, 1-20.

Carcione, J. M. and Tinivella, U., 2001, *The seismic response to overpressure: a modeling methodology based on laboratory, well and seismic data*, Geophys. Prosp., 49, 523-539.

Carcione, J. M. and Cavallini, F., 2002, *Poisson's ratio at high pore pressure*, Geophys. Prosp., 50, 97-106.

Chaney, P. E., 1950, *Abnormal pressure and lost circulation*:World Oil, 130, 122-126.

Chiarelli, A. and Duffaud, F., 1980, *Pressure origin and distribution in Jurassic of Viking basin (United Kingdom-Norway)*: AAPG Bulletin, 64, 1245-1266.

Childs, C., Manzocchi, T., Nell, P. A. R., Walsh, J. J., Strand, J. A., Heath, A. E., and Lygren, T. H., 2002, *Geological implications of a large pressure difference across a small fault in the Viking Graben, in Hydrocarbon Seal Quantification*. (Koestler, A. G. and Hunsdale, R., Eds.), Norwegian Petroleum Society (NPF), Special Publication, 11, 127-139.

Christensen, N. I., and Wang, H. F., 1985, *The influence of pore pressure and confining pressure on dynamic elastic properties of Berea sandstone*, Geophysics, 50, 207-213.

Dutta, N. C., 1983, *Shale compaction and abnormal pore pressures: A model of geopressures in the Gulf of Mexico Basin*, 53rd Ann, SEG Meeting.

Dutta, N. C., and Levin, F. K., 1990, *Geopressure, Geophysical Reprint Series No. 7*, Society of Exploration Geophysicists.

Domenico, S. N., 1977, *Elastic properties of unconsolidated porous sand reservoirs*, Geophysics, 42, 1339-1368.

Continued on Page 30

ROCK PHYSICS OF GEOPRESSURE AND PREDICTION OF ABNORMAL PORE FLUID PRESSURES USING SEISMIC DATA

Continued from Page 29

José M. Carcione was born in Buenos Aires, Argentina, in 1953. He received the degree "Licenciado; in Fisicas' from Buenos Aires University in 1978, the "Dottore in Fisica" from Milan University in 1984, and Ph.D. in Geophysics from Tel Aviv University in 1987. In 1987 he was awarded the Alexander von Humboldt scholarship for a position at the Geophysical Institute of Hamburg University, where he stayed from 1987 to 1989.

From 1978 to 1980 he worked at the " Comisión Nacional de Energfa Atómica" at Buenous Aires. From 1981 to 1987 he worked as a research geophysicist at "Yacimientos Petrolfferos Fiscales" the national oil company of Argentina. Presently, he is a senior geophysicist at the "Instituto Nazionale de Oceanografia et di Geofisica Sperimentale (OGS)" (former Osservatorio Geofisico Sperimentale) in Trieste, where he was Head of the Department of Geophysics from 1996 to 2000. He has been editor of GEOPHYSICS since 1999. His current research deals with numerical modeling, the theory of wave propagation in acoustic and electromagnetic media, and their application to geophysical problems.

Hans B. Helle, received his MSc (Oceanography) from University of Bergen (Norway) in 1973. From 1970 to 1977 he worked as a research fellow and assistant professor at Geophysical Institute (UoB), and in 1978-1980 as a research engineer at SINTEF, Trondheim. From 1980 to 1983 he was an assistant professor at Seismological Observatory (UoB). From 1984 to the present he has been a research geophysicist at Norsk Hydro, E & P Research Center, Bergen. He has written a number of papers on oceanography, seismology and seismic. His current interests are numerical modeling of seismic wave propagation in realistic media and its application to rock and fluid characterization from seismic data. One of his recent sidetracks is computational neural network applied to reservoir characterization from well logs. He is a member of SEG, EAGE and Association of Marine Researchers (Norway).

Dvorkin, J. and Walls, J. 2000, *Detecting overpressure from seismic velocity calibrated to log and core measurements, 32nd Annual Offshore technology conference*, Paper OTC 11912.

Eaton, B. A. 1976, *Graphical method predicts geopressure worldwide, World Oil*, July issue, 100-104.

Eaton, B. A., and Eaton, T. L., 1997, Fracture gradient prediction for the new *generation*, World Oil, October issue, 93-100.

Foster, J. B., and Whalen, J. E., 1966, *Estimation of formation pressures from electrical surveys Offshore Louisiana*, Journal of Petroleum Technology, February issue.

Gangi, A. F., and Carlson, R. L., 1996, *An asperity-deformation model for effective pressure*,Tectonophysics, 256, 241-251.

Gist, G. A., 1994, *Fluid effects on velocity and attenuation in sandstones*, J. Acoust. Soc. Am., 96, 1158-1173.

Goldberg, I., and Gurevich, B., 1998, *A semi-empirical velocity-porosity-clay model for petrophysical interpretation of P- and S- velocities*, Geophys. Prosp., 46, 271-285.

Harrold, T. W. D., Swarbick, R. E., and Goulty, N. R., 1999, *Pore pressure estimation from mudrock porosities in tertiary basins*, Southeast Asia, AAPG Bulletin, 83, 1057-1067.

Han, D., Nur, A., and Morgan, D., 1986, *Effects of porosity and clay content on wave velocities in sandstones*, Geophysics, 51, 2093-2107.

Hart, B. S., Flemings, P. B., and Desphande, A., 1995, *Porosity and pressure: role of compaction disequilibrium in the development of geopressures in a Gulf Coast Pleistocene basin*, Geology, 23.

Hashin, Z., and Shtrikman, S., 1963, *A variational approach to the elastic behavior of multiphase materials*, J. Mech. Phys. Solids, 11, 127-140.

Helle, H. B., Bhatt, A., and Ursin, B., 2001, *Porosity and permeability prediction from wireline logs using artificial neural networks*, A North Sea case study, Geophys. Prosp., 49, 431-444.

Helle, H.B. and Bhatt, A., 2002, *Fluid saturation from well logs using committee neural networks*: Petroleum Geoscience, 8, 109-118.

Holbrook, P., Maggiori, D. A., and Hensley, R., 1995, *Real time pore pressure and fracture pressure determination in all sedimentary lithologies*, SPE Formation Evaluation, December issue, 215-222.

Iverson, W. P., Martinsen, R. S., and Surdam, R. C., 1994,*Pressure seal permeability and two-phase flow*: AAPG Memoir 61, 313-319. The American Association of Petroleum Geologists.

Johnson, D. L., Koplik, J., and Dashen, R., 1987, *Theory of dynamic permeability and tortuosity in fluid-saturatedporous media*: J. Fluid Mech., 176, 379-402.

Kan, T. K., and Sicking, C. J., 1994, *Pre-drill geophysical methods for geopressure detection and evaluation in abnormal formation pressures*, Chapman, R. Ed., Elsevier, 155-186.

Keyser, W. Johnston, L. Reeses, R., and Rodriguez, G., 1991, *Pore pressure prediction from surface seismic*, World Oil, 212, September issue, 115-125.

King, M. S., Marsden, J. R., and Dennis, J. W., 2000, *Biot dispersion for P- and S-waves velocities in partially and fully saturated sandstones*, Geophys. Prosp., 48, 1075-1089.

Kjartansson, E., 1979, *Constant Q-wave propagation and attenuation*, J. Geophys. Res., 84, 4737-4748.

Knight, R., and Dvorkin, J., 1992, *Seismic and electrical properties of sandstones at low saturations*, J. Geophys. Res.,97, 17425-17432.

Koren, Z., Kosloff, D. Zackhem, U., and Fagin, S., 1998, *Velocity model determination by tomography of depth migrated gathers*, in S. Fagin, ed., Model-Based Depth Imaging, Society of Exploration Geophysicist, Course Note Series Nr. 10, 119-130.

Krief, M., Garat, J., Stellingwerff, J., and Ventre, J., 1990, *A petrophysical interpretation using the velocities of P and S waves (full waveform sonic)*, The Log Analyst, 31, 355-369.

Kuster, G. T., and Toksöz, M. N., 1974, *Velocity and attenuation of seismic waves in two-phase media: Part I.Theoretical formulations*, Geophysics, 39, 587-606.

Law, B. E., Ulmishek, G. F., and Slavin, V. I. (eds.), 1998, *Abnormal pressures in hydrocarbon environments*: AAPG Memoir 70. The American Association of Petroleum Geologists.

Leclaire, Ph., Cohen-Tenoudji, F., and Aguirre-Puente, J., 1994, *Extension of Biot's theory of wave propagation to frozen porous media*, J. Acoust. Soc. Am., 96, 3753-3768.

Lesso, W. G. Jr., and Burgess, T. M., 1986, *Pore pressure and porosity from MWD measurements*, IADC/SPE Drilling Conf., #14801.

Louis, J. N., and Asad, A. M., 1994, *Seismic amplitude versus offset (AVO) character of geopressured transition zones*: AAPG Memoir 61, 131-137. The American Association of Petroleum Geologists.

Luo, X., and Vasseur, G., 1996, *Geopressuring mechanism of organic matter cracking: numerical modeling*, AAPG Bull., 80, 856-874.

Mann, D. M., and Mackenzie, A. S., 1990, *Prediction of pore fluid pressures in sedimentary basins*: Marine and Petroleum Geology, 7, 55-65.

Mavko, G., Mukerji, T., and Dvorkin, J., 1998, *The rock physics handbook: tools for seismic analysis in porous media*, Cambridge Univ. Press.

Matusevich, V. M., Myasnikova, G. P., Maximov, A. M., Volkov, A. M., Christiakova, N. F., Kanalin, V.G. and Pupilli, M., 1997, *Abnormal formation pressure in the West*

Continued on Page 32

ROCK PHYSICS OF GEOPRESSURE AND PREDICTION OF ABNORMAL PORE FLUID PRESSURES USING SEISMIC DATA

Continued from Page 30

Siberian Mega-basin, Russia: Petroleum Geoscience, 3, 269-283.

Meissner, F. F., 1978, *Petroleum geology of the Bakken Formation, Williston Basin, North Dakota and Montana*: Montana Geol. Soc. Symp., 207-227.

Miley, M. P., 1999, *Converted modes in subsalt seismic exploration*, M.Sc., Thesis, Rice University.

Miley, M. P., and Kessinger, W. P., 1999, *Overpressure prediction using converted mode reflections from base of salt*, 60th Ann. Internat. Mtg., Soc.Expl. Geophys., Expanded Abstracts, 880-883.

Murphy, W. F., 1982, *Effect of partial water saturation on attenuation of Massilon sandstone and Vycor porous glass*, J. Acoust. Soc. Am., 71, 1458-1468.

Pennebaker, E., 1968, *Seismic data indicate depth and magnitude of abnormal pressures*, World Oil, 166, 73-78.

Pham, N. H., Carcione, J. M., Helle, H. B., and Ursin, B., 2002, *Wave velocities and attenuation of shaley sandstones as a function of pore pressure and partial saturation*. Geophys. Prosp.(in press).

Prasad, M., and Manghnani, M. H., 1997, *Effects of pore and differential pressure on compressional wave velocity and quality factor in Berea and Michigan sandstones*, Geophysics, 62, 1163-1176.

Rubey, W. W., and Hubbert, M. K., 1959, *Role of fluid pressure mechanics of overthrust faulting, II. Overthrust belt in geosynclinal area of Western Wyoming in light of fluid pressure hypothesis*, Geol. Soc. Am., 70, 167-205.

Sayers, C. M., Johnson, G. M., and Denyer, G., 2000, *Predrill pore pressure prediction using seismic data*, IADC/SPE Drilling Conf., #59122.

Schoenberg, M., and Muir, F., 1989, *A calculus for finely layered media*: Geophysics, 54, 582-590.

Smith, J. E., 1971, *The dynamics of shale compaction and evolution ofpore-fluid pressure*, Math. Geol., 3, 239-263.

Terzaghi, K., 1936, *The shearing resistance of saturated soils and the angle between the planes of shear, in: Proceedings of the International Conference on Soil Mechanics and Foundation Engineering*, Harvard University Press, Cambridge, 1, 54-56.

Todd, M. P., and Simmons, W. S., 1972, *Effect of pore pressure on the velocity of compressional waves in low-porosity rocks*, J. Geophys. Res., 70 (20), 3731-3743.

Tinivella, U., Carcione, J. M., and Helle, H. B., 2001, *Estimation of pore pressure by AVO inversion*, 71th Ann. Internat. Mtg., Soc. Expl. Geophys., Expanded Abstracts (CD-rom).

Traugott, M.,1997, *Pore/fracture pressure determinations in deep water, Deepwater Technology supplement*, World Oil, 218 August issue.

Vernik, L., 1994, *Hydrocarbon-generation-induced microcraking of source rocks*, Geophysics, 59, 555-563.

Vernik, L., 1995, *Petrophysics of the Kimmeridge shale, North Sea*, Stanford Rock Physics Laboratory.

Vernik, L. and Nur A., 1992, *Ultrasonic velocity and anisotropy of hydrocarbon source rocks*, Geophysics, 57, 727-735.

Vernik, L. and Landis, C., 1996, *Elastic anisotropy of source rocks: implications for hydrocarbongeneration and primary migration*: AAPG Bulletin, 80, 531-544.

Winkler, K. W., 1985, *Dispersion analysis of velocity and attenuation in Berea sandstone*, J. Geophys. Res., 90, 6793-6800.

Yin, C. S., Batzle, M. L., and Smith, B. J., 1992, *Effects of partial liquid/gas saturation on extensional wave attenuation in Berea sandstone*, Geophys. Res. Letters, 19, 1399-1402.

Zimmerman, R. W., 1991, *Compressibility of sandstones*,Elsevier, New York, R

Editorial Calendar 2002-2003

Issue	Due date		Theme
2002	October	August 31st	**Natural Gas Hydrates**
	November	September 30th	**Lessons from the School of Hard Rocks**
	December	October 31st	**The latest from the field: issues, developments and technology**
2003	January	November 30th	**Just beneath the surface – shallow geophysical applications**
	February	December 31st	**A look at Geophysics from around the world**
	March	January 31st	**Future of Geophysics — a look at leading edge university research**
	April	February 29th	**A focus on statics: what are the problems, how are we solving them?**
	May	March 31st	**Major geological regimes – an overview**
	June	April 30th	**Exciting new research being done in deep crustal studies**